Prior to Undergoing Epithelial to Mesenchymal Transition, Premalignant Cells Transiently Increase Tensile Forces at Cell-Cell and Cell-Matrix Adhesions

Lídia Faria± (1, 2, 3), Carine M Gonçalves± (1, 2), Inês Fidalgo (1, 2, 4), Carla S. Lopes (1, 5); Vanessa Rodrigues (1,2); Maria M. Azevedo (1, 5); Paula Sampaio (1, 5); Sandra Tavares (1, 2); Vaibhav Mahajan (6); Anna Taubenberger (6); and Florence Janody* (1, 2)

(1) Instituto de Investigação e Inovação em Saúde (i3S), Universidade do Porto, Rua Alfredo Allen, 208, 4200-135 Porto, Portugal.
(2) Instituto de Patologia e Imunologia Molecular da Universidade do Porto (Ipatimup), Rua Júlio Amaral de Carvalho, n 45, 4200-135 Porto, Portugal.
(3) Doctoral Programme in Molecular and Cell Biology, School of Medicine & Biomedical Sciences, University of Porto (ICBAS-UP), Rua Jorge Viterbo Ferreira 228, 4050-513 Porto, Portugal.
(4) Master Programme in Oncology, School of Medicine & Biomedical Sciences, University of Porto (ICBAS-UP), Rua Jorge Viterbo Ferreira 228, 4050-513 Porto, Portugal.
(5) Instituto de Biologia Molecular e Celular (IBMC), Universidade do Porto, Rua Alfredo Allen 208, 4200-135, Porto, Portugal.
(6) Biotechnology Center, Technische Universität Dresden, Tatzberg 47/49, 01307 Dresden, Germany.

±These authors contributed equally to this work.
*corresponding author:
e-mail: fjanody@i3s.up.pt
Tel. (+351) 22 557 0730

Running Title: Forces at cell adhesion sites in cellular transformation

Key words: Adherens Junctions/Focal Adhesions//Mechanotransduction/Src proto-oncogene/cancer progression

Abstract

The weakening of Adherens Junctions (AJs) and Focal Adhesions (FAs) adhesiveness has been proposed to enable the initiation and progression of several types of cancer. Here we report that, prior to disassembling AJs and acquiring malignant traits, premalignant mammary epithelial cells overactivating the Src proto-oncogene transiently enhance tensile forces at both AJs and FAs, thereby gaining a proliferative advantage. We show that AJs and FAs are transiently under higher tensile forces in premalignant Src-activated cells. Cells unable to increase tensile forces at FAs by knocking down PXN or inhibiting FAK activity fail to transiently build up tensile force at AJs and to grow. Conversely, preventing AJ strengthening using EGTA or small interference RNA against P-cadherin suppresses the transient increase in tensile forces at FAs, EGFR-ERK and MRTF-A-SRF activation and cell proliferation. Moreover, knocking down E-cadherin, the sole classical cadherin in *Drosophila*, inhibits Src-induce tissue overgrowth *in vivo*. Thus, prior to the loss of cell-cell and cell-matrix adhesiveness, strengthening of AJs and FAs may be an essential early step for mammary cells to gain a proliferative advantage and establish the mechanical and signaling conditions necessary for subsequent malignant transformation.

Statement of Significance

Although the weakening of cell-cell and cell-matrix adhesiveness is commonly associated with cancer initiation and progression, our findings reveal that an initial increase in adhesiveness enables proliferation and malignant progression.

52 **Introduction**

53 Most breast cancers arise in the epithelial ducts and are referred to as ductal carcinoma. The
54 most acknowledged model of ductal breast cancer progression states that every invasive
55 carcinoma originates from a benign hyperplasia. These lesions are caused by excessive
56 proliferation of the terminal duct lobular units, leading to dilated ducts, lined with one or more
57 layers of epithelial cells (1). Progression of these proliferative breast lesions to invasive
58 carcinoma has been proposed to involve a shift from an epithelial to a mesenchymal phenotype,
59 in a process referred to as Epithelial to Mesenchymal Transition (EMT), characterized by the
60 breakdown of Adherens Junctions (AJs) and dynamic remodeling of Focal Adhesions (FAs)
61 (2).

62 AJs are the major cell-cell adhesion structure that senses and responds to tensile forces at the
63 intercellular contact interface and hold epithelial cells together (3). AJs assemble through
64 homotypic interactions between the extracellular domains of classical cadherins from adjacent
65 cells in a Ca^{2+}-dependent manner. E-cadherin (Ecad) is one of the main classical cadherins,
66 highly conserved from bilaterian metazoans to mammals and expressed in most epithelial
67 tissues (4). Intracellularly, the Ecad cytoplasmic tail interacts with p120-catenin (p120ctn) and
68 β-catenin (βcat). While p120ctn promotes the assembly of Ecad dimers, βcat interacts with the
69 actin-binding protein α-catenin (αcat) and physically links AJ complexes to the actomyosin
70 cytoskeleton in a force-dependent manner (5). P-cadherin (Pcad), another classical cadherin, is
71 also expressed in several epithelia, where it can overlap with Ecad. Alike Ecad, Pcad promotes
72 cell-cell adhesion and Ca^{2+}-dependent cell-cell aggregation (6).

73 At the cell-extracellular matrix (ECM) interface, mechanosensitive FAs assemble from nascent
74 adhesions, which form upon the binding of a few integrin dimers to their ECM ligands and to
75 Talin intracellularly (7). The coupling of integrins to the actomyosin cytoskeleton through
76 Talin and Paxillin recruits Vinculin, leading to the maturation of nascent adhesions into larger
77 and more stable FAs. The mechanisms in play involve the stretching of Talin and Vinculin by
78 tensile forces, thereby re-enforcing the connection between integrins and the actomyosin
79 cytoskeleton and the recruitment of additional proteins, including Focal Adhesion Kinase
80 (FAK) and Zyxin to stress fiber-bound FAs (8,9). Thus, Ecad and Vinculin are *bona fide*
81 mechanosensors (9,10).

82 In addition to maintaining cell–cell contact and attachment to the ECM, piconewton
83 mechanical forces transmitted at AJs and FAs expose cryptic sites within mechanosensitive
84 proteins and modulate the binding kinetics of receptor-ligand complexes to regulate the activity
85 of diverse mechanotransduction signaling pathways and therefore cell behavior (11).

86 Mechanical forces associated with FAs induce the nuclear translocation of the myocardin-
87 related transcription factor (MRTF-A), a co-factor of serum response factor (SRF), which
88 triggers invasion in mammary epithelial cells (12). Likewise, ECM-dependent FA
89 strengthening promotes mammary epithelial cell growth through activation of extracellular
90 signal-regulated kinase (ERK) (13). Increasing tension on homophilic Ecad bonds has also
91 been shown to stimulate ERK-dependent proliferation by enabling the homodimerization of
92 epidermal growth factor receptor (EGFR) in A-431D epithelial cells (14). Forces on AJs can
93 also be transferred to FAs and *vice versa*. Integrin engagement or higher traction force from
94 the ECM can increase tension at cell-cell contacts in multiple cell types (15,16). Conversely,
95 Ecad force transmission increases the average FA area and number and Myosin-dependent cell
96 contractility in MCF7 cells (17). In turn, integrins strengthen tensile forces at AJs, thus,
97 establishing a positive mechanotransduction feedback loop between force-activated Ecad and
98 integrins (18). However, strengthening of one adhesion can also antagonize the assembly of
99 the other (11). How the balance of forces between adhesion sites controls distinct outcomes
100 during cancer progression is not fully understood.
101 Using the mammary epithelial cells MCF10A-ER-Src (ER-Src), which contains a fusion
102 between the non-receptor tyrosine kinase v-Src and the ligand-binding domain of the Estrogen
103 Receptor (ER-Src), inducible with tamoxifen (TAM) treatment, we have reported that
104 malignant progression involves two main phases. During the first 12 hours of Src activation,
105 cells acquire a phenotypic state akin to premalignant cells, characterized by the gain of
106 proliferative abilities, which depends on a transient increase in cell stiffening, and activation
107 of ERK and MRTF-A/SRF signaling in cells that maintain an epithelial-like organization. 24
108 hours after Src activation, cells progress into a malignant phase, defined by the loss of
109 epithelial-like organization associated with the downregulation of Ecad and Pcad and the
110 upregulation of the EMT transcription factor SNAIL1 (19-21). We now provide evidence that
111 the prior disassembling their AJs, premalignant ER-Src cells transiently increase tensile forces
112 at AJs and FAs to acquire a proliferative advantage. Thus, tensile forces at AJs and FAs could
113 have paradoxical roles during tumor progression. Strengthening of AJs and FAs may be an
114 essential early step for premalignant breast cells to gain a proliferative advantage and establish
115 the mechanical and signaling conditions necessary for subsequent malignant transformation.
116 In contrast, the later weakening of forces at AJs and FAs could facilitate the emergence of
117 malignant behaviors such as loss of adhesion, increased motility, and invasiveness.

118 **Results**

119

120 **Src strengthens tensile forces at AJs prior to inducing EMT**

121 Prior to acquiring malignant features, premalignant ER-Src cells turn transiently stiffer (19).
122 We therefore asked if AJs were under higher tension in TAM-treated ER-Src cells. To this end,
123 we generated ER-Src cells stably expressing an Ecad fluorescence resonance energy transfer
124 (FRET)-based tension sensor (Ecad-TS), known to respond to changes in tensile forces at cell-
125 cell contacts (10). The Ecad-TS was built by inserting a tension module (TS), containing a
126 flagelliform elastic linker flanked by the mTFP1 donor and Venus acceptor fluorescent proteins
127 in the Ecad coding sequence, between the transmembrane domain and the catenin-binding
128 domain (Fig. 1A). As expected, the Ecad-TS was recruited at cell-cell contacts where it co-
129 localized with p120ctn (Fig. 1B). To ensure that the Ecad-TS was functional, we tested if
130 expressing the Ecad-TS in MDA-MB-231 cells that lack Ecad, restored cell-cell contacts. While
131 p120ctn was barely detectable in control MDA-MB-231 cells, those expressing the Ecad-TS
132 recruited p120ctn at the membrane between adjacent Ecad-TS expressing MDA-MB-231 cells
133 and acquired a cobblestone-like shape (Fig. 1C). We next assessed if tensile forces applied to
134 the Ecad-TS were altered during transformation of ER-Src cells by performing fluorescence
135 lifetime measurement (FLIM) of the Ecad-TS donor, a quantitative imaging technique that is
136 less sensitive to imaging or processing artifacts than the FRET ratio-metric approach (22). For
137 FLIM analysis we focused on donor's lifetimes, which increases as the distance with the
138 acceptor increases. This approach revealed that the donor lifetime of the Ecad-TS was
139 significantly extended in ER-Src cells treated with TAM for 6 or 12 hours, compared to those
140 treated with the vehicle EtOH for the same time (Fig. 1D), suggesting that AJs are under higher
141 tension in premalignant ER-Src cells. While cells undergo EMT 24 hours after TAM treatment
142 (21), those that still maintained cell-cell contacts retained an extended donor lifetime of the
143 Ecad-TS (Fig. 1D). To ensure that alterations of the Ecad-TS donor lifetime in TAM-treated
144 cells resulted from higher tensile forces on Ecad, we also generated ER-Src cells expressing a
145 control Ecad-TS construct lacking the βcat–binding domain (Ecad-TSΔcyto), which therefore
146 cannot associate with F-actin (Fig. 1A). Ecad-TSΔcyto localized with p120ctn at cell-cell
147 contacts in ER-Src cells (Fig. 1B), but did not recruit p120ctn at the cell membrane in MDA-
148 MB-231 cells (Fig. 1C). The donor lifetime of the Ecad-TSΔcyto was not affected between
149 EtOH and TAM-treated cells at any time point (Fig. 1E), indicating that the extended donor
150 lifetime of the Ecad-TS in TAM-treated ER-Src cells depends on its ability to interact with the
151 actin cytoskeleton. The Ecad-TS donor lifetime also depends on Myosin II activity, as

Blebbistatin significantly lowered the Ecad-TS donor lifetime in cells treated with EtOH or TAM for 6 hours, compared to those grown in the absence of Blebbistatin (Supp. Fig. 1A).

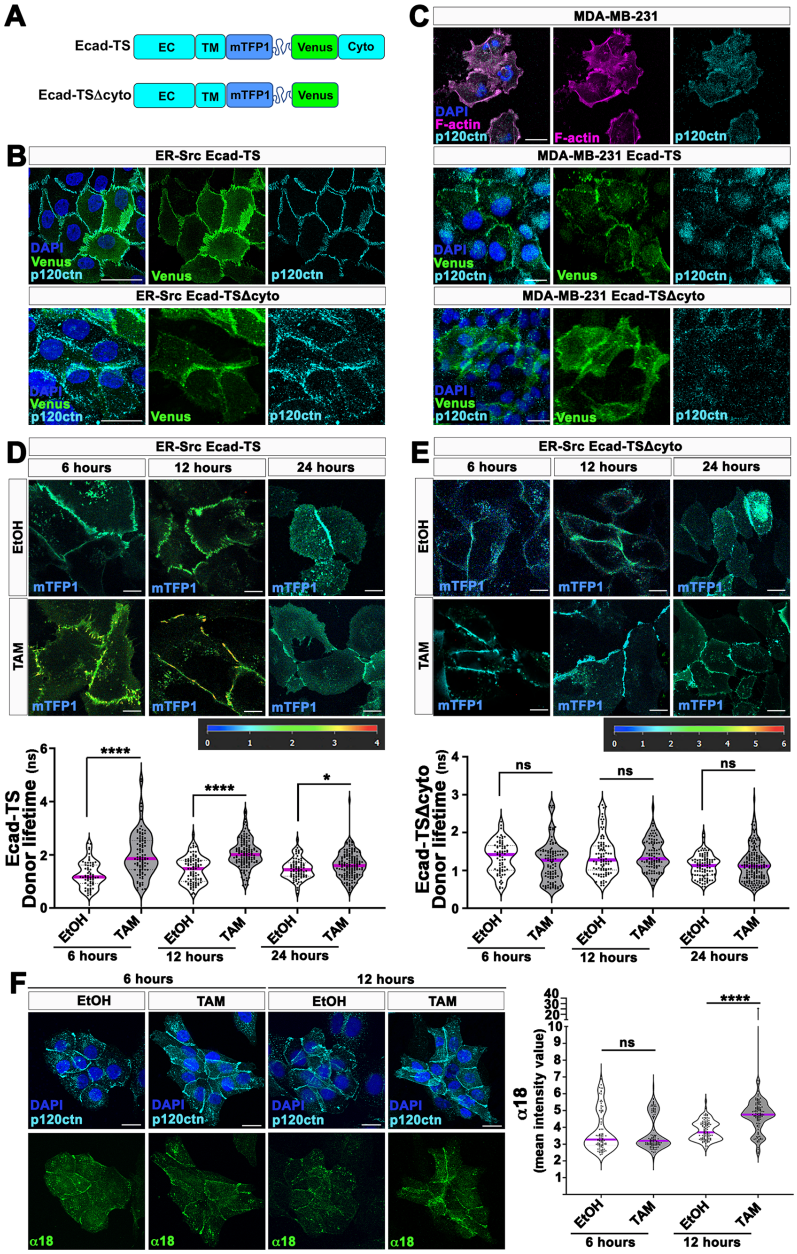

Figure 1: Prior to undergoing EMT, TAM-treated ER-Src cells strengthen tensile forces at AJs. (A) Schematics of the Ecad-TS and Ecad-TSΔcyto. EC: extracellular domain; TM transmembrane domain; cyto: cytoplasmic domain. **(B)** Confocal images of ER-Src cells expressing the Ecad-TS (Venus in green) or Ecad-TSΔcyto (Venus in green) and stained with anti-p120ctn (cyan) and DAPI (blue). **(C)** Confocal images of MDA-MB-231 cells, stained with anti-p120ctn (cyan), Phalloidin (magenta) and DAPI (blue) or expressing Ecad-TS (Venus in green) or Ecad-TSΔcyto (Venus in green), and stained with anti-p120ctn (cyan) and DAPI (blue). **(D)** (Top) ER-Src cells expressing Ecad-TS and treated with EtOH or TAM for 6, 12 or 24 hours. Color bar indicates 0–4 ns. (Bottom) Quantification of the mTFP1 lifetime at cell-cell contacts in ER-Src cells expressing the Ecad-TS and treated with EtOH or TAM for 6, 12 or 24 hours. **(E)** (Top) ER-Src cells expressing the Ecad-TSΔcyto and treated with EtOH or TAM for 6, 12 or 24 hours. Color bar indicates 0–6 ns. (Bottom) Quantification of the mTFP1

167 lifetime at cell-cell contacts in ER-Src cells expressing the Ecad-TSΔcyto and treated with
168 EtOH or TAM for 6, 12 or 24 hours. Higher and lower donor lifetime correspond to higher and
169 lower tension, respectively. **(F)** (Left) Confocal images of ER-Src cells treated with EtOH or
170 TAM for 6 or 12 hours and stained with the α18 antibody (green), anti-p120ctn (cyan) and
171 DAPI (blue). (Right) Quantification of the α18 mean intensity levels at cell-cell contacts in
172 ER-Src cells treated with EtOH or TAM for 6 or 12 hours. Quantifications are from three
173 biological replicates and are presented as violin plots with the magenta lines indicating median
174 values. Statistical significance was calculated using Mann – Whitney t-tests. ns indicates non-
175 significant. *P<0.05; ****P<0.0001. Scale bars represent 20 μm.

176

177 To confirm that prior to disassembling AJs 24 hours after TAM treatment, AJs are under higher
178 tension, we stained cells with an antibody against the α18 epitope of αcat, a cryptic site revealed
179 when tension is applied at AJs (23). While the intensity of the α18 antibody at cell-cell contacts
180 was not significantly different between ER-Src cells treated with EtOH or TAM for 6 hours, it
181 was significantly higher in cells treated with TAM for 12 hours, compared to those treated with
182 EtOH for the same time (Fig. 1F). Because total αcat levels were not affected between EtOH
183 and TAM-treated cells (Supp. Fig. 1B and C), we conclude that AJs are under higher tension in
184 premalignant ER-Src cells, prior cells disassembling AJs.

185

186 **FAs are transiently under higher tension in premalignant ER-Src cells**

187 Premalignant ER-Src cells accumulate polarized FA-associated stress fibers (19). We therefore
188 asked if tension at FAs was also affected in premalignant ER-Src cells. We generated ER-Src
189 cells expressing a Vinculin tension sensor (Vin-TS), which contains the tension module inserted
190 between the head domain that recruits Vinculin to FAs and the tail domain, which binds to the
191 mechanotransduction force machinery and responds to change in tension at FAs (9). To
192 abrogate the ability of the Vin-TS to respond to tension, we also generated stable ER-Src cells
193 expressing a Vin-TS lacking the tail domain (Vin-TSΔtail) (Fig. 2A). Vin-TS and Vin-TSΔtail
194 mainly localized with Zyxin at FAs (Fig. 2B). FRET-FLIM analysis indicated that the donor
195 lifetime of the Vin-TS at FAs was slightly extended 6 hours after TAM treatment, compared to
196 those treated with EtOH for the same time. This effect was strongly enhanced 12 hours after
197 TAM-treatment. However, 24 hours after treatment, this differential behavior was lost between
198 EtOH- and TAM-treated cells (Fig. 2C). In contrast, the donor lifetime inVin-TSΔtail was not
199 altered between EtOH- and TAM-treated cells at any time point (Fig. 2D). Moreover,
200 Blebbistatin reduced the donor lifetime of the Vin-TS 12 hours after EtOH or TAM treatment
201 (Supp. Fig. 2), indicating that the extended donor lifetime of the Vin-TS in TAM-treated ER-
202 Src cells depends on Myosin II activity.

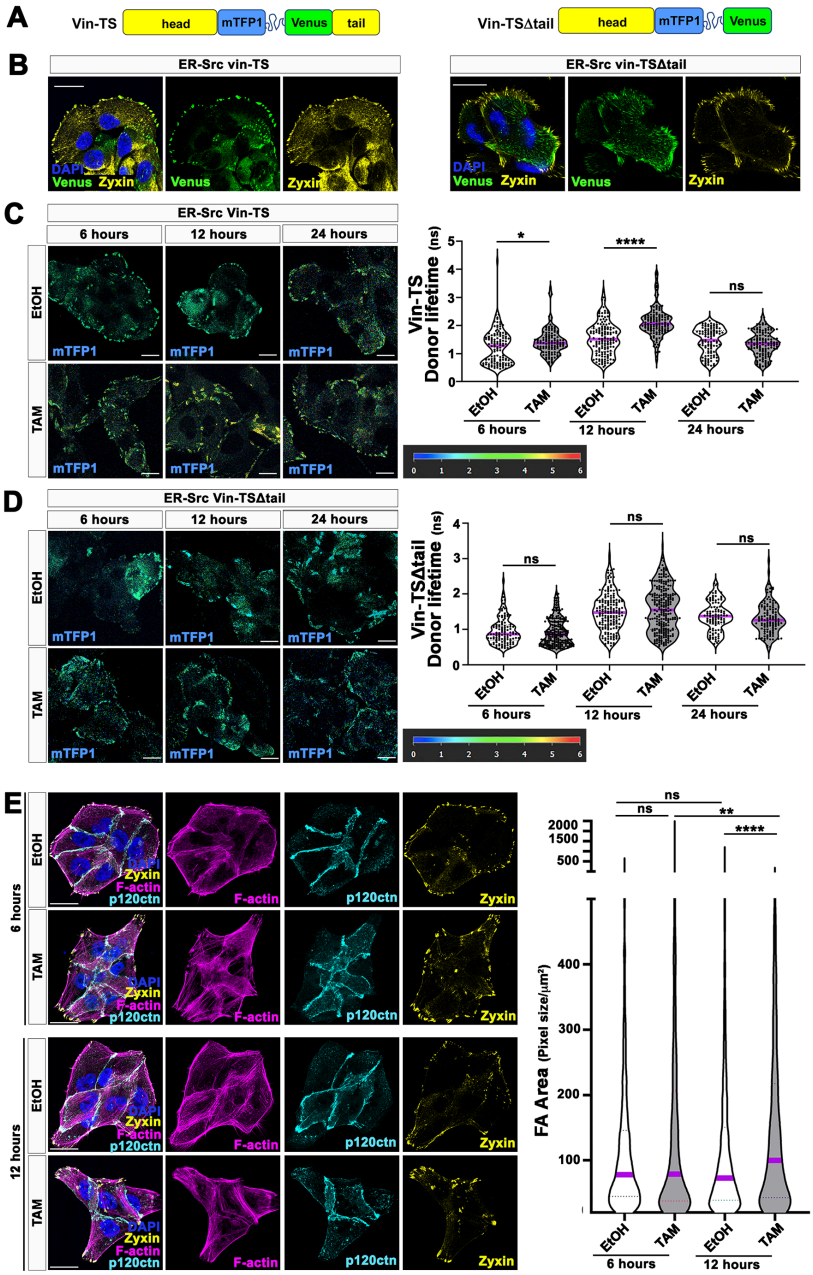

Figure 2: FAs are larger and transiently under higher tension in ER-Src cells. (A) Schematics of the Vin-TS and Vin-TSΔtail. **(B)** Confocal images of ER-Src cells expressing the Vin-TS (Venus in green) or Vin-TSΔtail (Venus in green) and stained with anti-Zyxin (yellow) and DAPI (blue). **(C)** (Left) ER-Src cells expressing the Vin-TS and treated with EtOH or TAM for 6, 12 or 24 hours. Color bar indicates 0–6 ns. (Right) Quantification of the mTFP1 lifetime at FAs in ER-Src cells expressing the Vin-TS and treated with EtOH or TAM for 6, 12 or 24 hours. Higher and lower donor lifetime correspond to higher and lower tension, respectively. **(D)** (Left) ER-Src cells expressing the Vin-TSΔtail and treated with EtOH or TAM for 6, 12 or 24 hours. Color bar indicates 0–6 ns. (Right) Quantification of the mTFP1 lifetime at FAs in ER-Src cells expressing the Vin-TSΔtail and treated with EtOH or TAM for 6, 12 or 24 hours. **(E)** (Left) Confocal images of ER-Src cells treated with EtOH or TAM for 6, or 12 hours, stained with Phalloidin (magenta), anti-Zyxin (yellow) and anti-p120ctn (cyan). (Right) Quantification of FA area in ER-Src cells treated with EtOH or TAM for 6 or 12 hours. Quantifications are from three biological replicates and are presented as violin plots with the magenta lines indicating median values. Statistical significance was calculated using Mann –

219 Whitney t-tests. ns indicates non-significant. *P<0.05; **P<0.01; ****P<0.0001. Scale bars
220 represent 20 μm.
221
222 High tension across Vinculin has been associated with FA enlargement (9). Thus, to confirm
223 that FAs are under higher tension in premalignant ER-Src cells, we evaluated the size of Zyxin-
224 positive area 6 and 12 hours after EtOH or TAM treatment (Fig. 2E). Quantifications indicated
225 that the average area of Zyxin puncta was significantly larger in ER-Src cells treated with TAM
226 for 12 hours, compared to those treated with EtOH for the same time (Fig. 2E), suggesting that
227 ER-Src cells assemble larger FAs 12 hours after TAM treatment. Together, we conclude that
228 FAs are under higher tension in premalignant ER-Src, prior cells undergoing EMT.
229
230 **Tension at FAs is required to strengthen forces at AJs in premalignant ER-Src cells**
231 Forces on FAs can be transferred to AJs (11). We therefore asked if preventing the transient
232 increase in tension at FAs suppressed the ability of premalignant ER-Src cells to increase
233 tension at AJs. We first tested the effect of inhibiting the activity of FAK, as FAK plays a key
234 role in building up tensile forces at FAs (24). Consistent with previous report (21), FAK
235 phosphorylation (pFAK) was strongly potentiated after 12 hours of treatment with TAM (Supp.
236 Fig. 3A). Blocking FAK phosphorylation with PF-573228, a known FAK inhibitor (FAKi),
237 strongly reduced pFAK levels in cells treated with either EtOH or TAM for 12 hours, compared
238 to those treated with DMSO (Supp. Fig. 3A). Inhibiting FAK activity did not prevent the
239 assembly of FAs, seen by the presence of Zyxin and Vin-TS-positive foci in ER-Src cells co-
240 treated with FAKi and EtOH or TAM (Fig. 3A). However, FAK activity is required for
241 strengthening tensile forces at FAs in premalignant cells, as the extended Vin-TS donor lifetime
242 at FAs 12 hours after TAM treatment was suppressed in the presence of FAKi. In contrast,
243 FAKi did not affect the Vin-TS donor lifetime in EtOH-treated cells (Fig. 3B).
244 We then tested if inhibiting FAK activity affected tension at AJs. ER-Src cells co-treated with
245 FAKi and EtOH or TAM for 12 hours still assembled in clusters with p120ctn and the Ecad-TS
246 localized at the interface between neighboring cells (Fig. 3C). However, FAKi prevented the
247 extended Ecad-TS donor lifetime at AJs in TAM-treated ER-Src cells at 12 hours (Fig. 3D).
248 Moreover, FAKi significantly suppressed the growth of TAM-treated cells at 48 hours (Fig.
249 3E), but had no major effect on cell viability (Fig. 3F), indicating that FAK activation provides
250 a proliferative advantage to TAM-treated ER-Src cells.

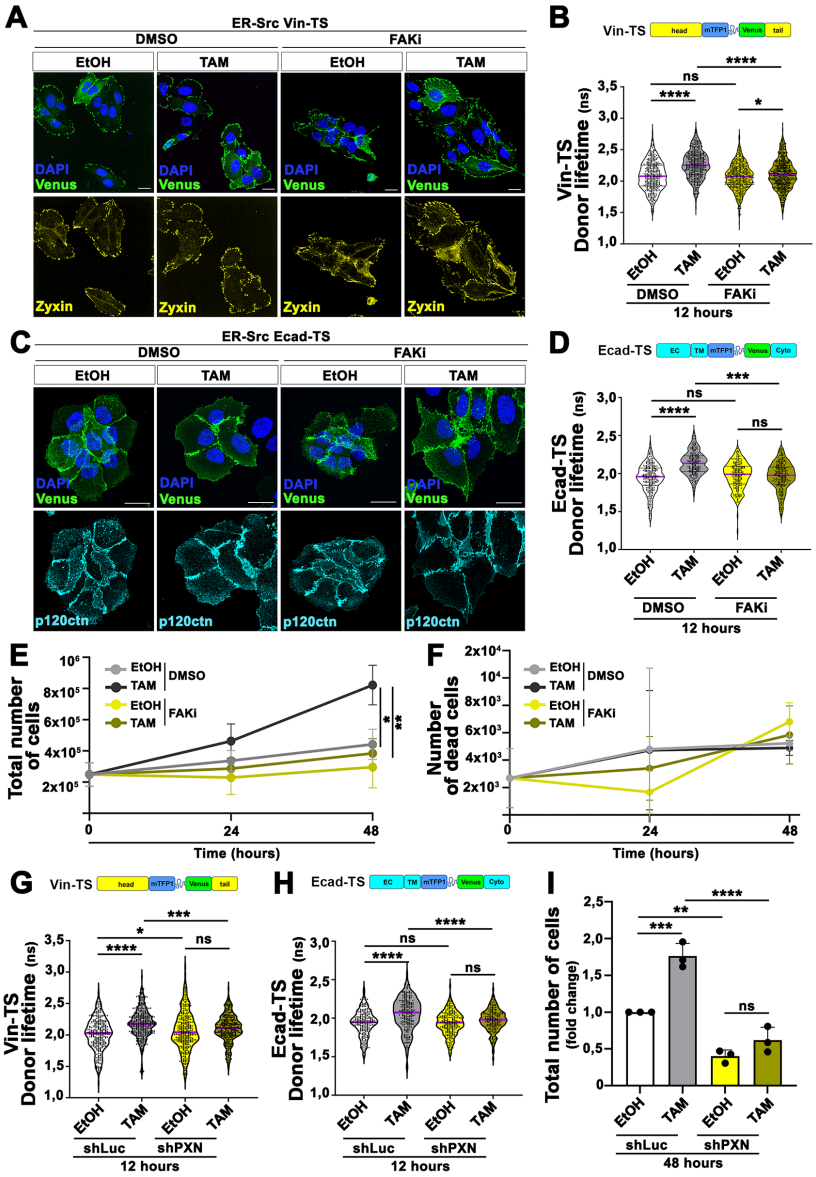

Figure 3: TAM-treated ER-Src cells lose the ability to increase tensile forces at AJs and to grow when unable to strengthen forces at FAs. (A) Confocal images of ER-Src cells expressing the Vin-TS (Venus in green) and co-treated with EtOH or TAM and DMSO or FAKi for 12 hours. Cells are stained with anti-Zyxin (yellow) and DAPI (blue). **(B)** Quantification of the mTFP1 lifetime at FAs in ER-Src cells expressing the Vin-TS and co-treated with EtOH or TAM and DMSO or FAKi for 12 hours. **(C)** Confocal images of ER-Src cells expressing the Ecad-TS (Venus in green) and co-treated with EtOH or TAM and DMSO or FAKi for 12 hours. Cells are stained with anti-p120ctn (cyan) and DAPI (blue). **(D)** Quantification of the mTFP1 lifetime at AJs in ER-Src cells expressing the Ecad-TS and co-treated with EtOH or TAM and DMSO or FAKi for 12 hours. Quantifications of donor lifetime are presented as violin plots with the magenta lines indicating median values. Scale bars represent 20 µm**. (E)** Growth curve of ER-Src cells co-treated with EtOH or TAM and DMSO or FAKi during 48 hours. **(F)** Quantification of dead ER-Src cells co-treated with EtOH or TAM and DMSO or FAKi at 24h and 48h timepoints. **(G)** Quantification of the mTFP1 lifetime at FAs in ER-Src cells expressing the Vin-TS and shLuc or shPXN and treated with EtOH or TAM for 12 hours. **(H)** Quantification of the mTFP1 lifetime at AJs in ER-Src cells expressing the Ecad-TS and shLuc or shPXN and treated with EtOH or TAM for 12 hours. **(I)** Quantification of the total number of ER-Src cells expressing shLuc or shPXN and treated with

270 EtOH or TAM for 48 hours. Quantifications are from three biological replicates. Statistical
271 significance was calculated using one-way ANOVA with Tukey's multiple comparison. ns
272 indicate non-significant. *P<0,05; **P<0.01; ***P<0.001; ****P<0.0001.
273
274 To confirm that increased tension at FAs strengthens forces at AJs and is required for cellular
275 transformation, we knocked down PXN using small-hairpin RNAs (shPXN), as Paxillin is one
276 of the consensus FA components, not shared between AJs and FAs (11,25). EtOH or TAM-
277 treated ER-Src cells expressing shPXN showed reduced Paxillin protein levels, compared to
278 those infected with small-hairpin RNAs against Luciferase (shLuc), used as control (Supp. Fig.
279 3B). Knocking down PXN in ER-Src cells did not prevent the assembly of Zyxin- and Vin-TS-
280 positive FAs (Supp. Fig. 3C). It did not either induce the loss of cell-cell contacts, as Ecad was
281 still localized between adjacent PXN-depleted cells or between PXN-depleted cells and those
282 expressing Paxillin (Supp. Fig. 3D). However, knocking down PXN suppressed the extended
283 donor lifetime of the Vin-TS (Fig. 3G) and of the Ecad-TS (Fig. 3H) in cells treated with TAM
284 for 12 hours. Moreover, PXN-depleted cells showed a growth impairment, compared to those
285 expressing shLuc (Fig. 3I). Thus, we conclude that the transient strengthening of FAs in
286 premalignant ER-Src cells is required to increase tension at AJs and to sustain cell growth.
287
288 **Premalignant ER-Src cells unable to assemble AJs fail to strengthen tension at FAs.**
289 We then tested if, in turn, tension at AJs was transferred to FAs in premalignant ER-Src cells.
290 To this end, we disrupted cell-cell adhesion using the calcium chelator EGTA, which prevents
291 *trans* junctional homophilic interactions between cadherin extracellular domains (26). Thirty
292 minutes of EGTA treatment was sufficient to induce cell rounding and the loss of cell-cell
293 contacts in ER-Src cells (Supp. Fig. 4A). After removal of EGTA from the media, cells
294 remained viable for at least 24 hours (Supp. Fig. 4B), and recovered a cobblestone-like shape,
295 with p120ctn localized at cell-cell contacts (Supp. Fig. 4A). This shows that the EGTA-
296 dependent loss of cell-cell contacts is reversible. Thus, we first tested if EGTA affected the
297 size of FAs 12 hours after TAM treatment. As expected, ER-Src cells co-treated with EGTA
298 and EtOH or TAM for 12 hours maintained a rounder shape with E-cad poorly recruited at cell-
299 cell contacts, compared to those grown in the absence of EGTA (Fig. 4A). Quantification of
300 the size of Zyxin-positive puncta indicates that EGTA treatment significantly reduced the
301 average area of Zyxin-positive FAs in both EtOH- and TAM-treated cells (Fig. 4B). Thus,
302 tension at AJs could be required to strengthen forces on FAs. Accordingly, FLIM-FRET on the
303 Vin-TS indicates that the extended donor lifetime 12 hours after TAM treatment was

suppressed in the presence of EGTA. In contrast, EGTA had no major effect on the Vin-TS donor lifetime in EtOH-treated cells (Fig. 4C). EGTA treatment also prevented the transient increase in cell stiffening 6 hours after TAM treatment (Fig. 4D). Taken together, these observations suggest that higher tension exerted between TAM-treated ER-Src cells through cadherins, reinforces cortical tension and increases tensile forces at FAs.

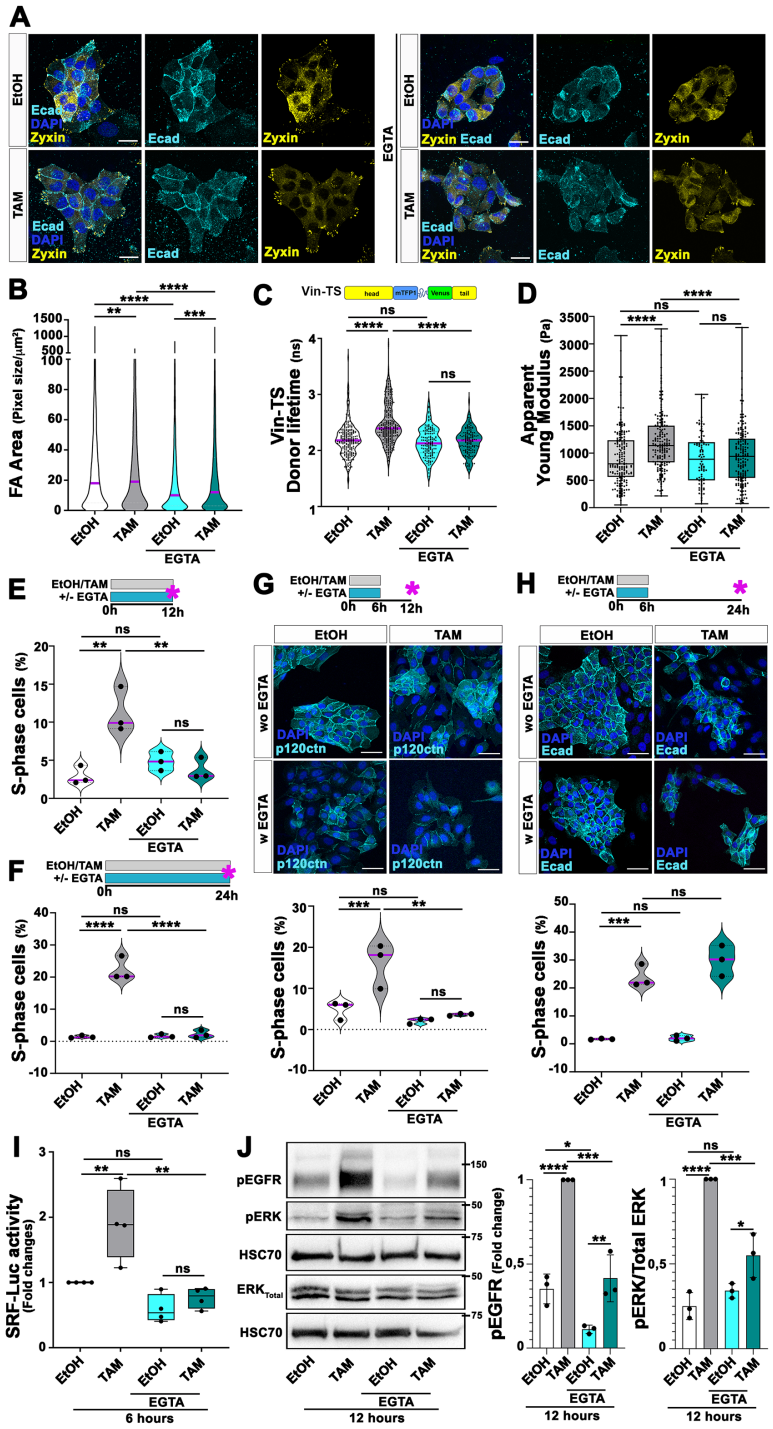

Figure 4: EGTA treatment hampers the ability of TAM-treated ER-Src cells to increase tension at FAs and to acquire sustained proliferative ability. (A) Confocal images of ER-

312 Src cells treated with EtOH or TAM for 12 hours in the presence or absence of EGTA, stained
313 with anti-Ecad (cyan), anti-Zyxin (yellow) and DAPI (blue). **(B)** Quantification of FA area in
314 ER-Src cells treated with EtOH or TAM for 12 hours in the presence or absence of EGTA. **(C)**
315 Quantification of the mTFP1 lifetime at FAs in ER-Src cells expressing the Vin-TS and treated
316 with EtOH or TAM for 12 hours in the presence or absence of EGTA. **(D)** Quantification of
317 the Apparent Young's modulus of ER-Src cells treated with EtOH or TAM for 6 to 8 hours in
318 the presence or absence of EGTA. (**E-H)** (Top) Schematics of the experimental designs.
319 Magenta stars indicate the time points at which cells were collected. (Bottom) Quantification
320 of the percentage of ER-Src cells in S-phase, in cells treated with EtOH or TAM hours in the
321 presence or absence of EGTA for **(E)** 12 hours or **(F)** 24 hours. **(G-H)** (Middle) confocal
322 images or (lower) quantifications of the percentage of cells in S-phase in ER-Src cells treated
323 with EtOH or TAM for 6 hours in the presence or absence of EGTA and left to grow for an
324 additional 6 **(G)** or 18 **(H)** hours in the absence of treatment. Cells are stained with Ecad (cyan)
325 and DAPI (blue). **(I)** Quantification of the fold changes in Luciferase activity in ER-Src cells
326 transfected with the SRF-responsive-Luc reporter gene and treated with EtOH or TAM for 6
327 hours in the presence or absence of EGTA. **(J)** (Left) Western blots on protein extracts from
328 ER-Src cells treated with EtOH or TAM for 12 hours in the presence or absence of EGTA,
329 blotted with anti-pEGFR, anti-pERK and anti-HSC70 used as loading control (middle) or anti-
330 ERK (ERK_{Total}) and anti-HSC70 (bottom). (Right) Quantifications of pEGFR levels or the ratio
331 of pERK over total ERK levels, normalized to HSC70 for the conditions indicated.
332 Quantifications are from three (B to H and J) or four (I) biological replicates and presented as
333 violin plots with the magenta lines indicating median values (B, C and E to H) or as column
334 plots (D, I and J). Statistical significance was calculated using a linear mixed model. ns indicate
335 non-significant. *<0.05; **P<0.01; ***P<0.001; ****P<0.0001. Scale bars indicate 20 µm.

336

337 **Premalignant ER-Src cells unable to assemble AJs fail to sustain proliferation.**

338 We then tested the consequences of preventing AJ assembly on the ability of TAM-treated ER-
339 Src cells to gain sustained proliferative abilities. Consistent with previous reports (19,20),
340 TAM-treated ER-Src cells showed a significant higher number of cells in S-phase of the cell
341 cycle, 12 (Fig. 4E) and 24 (Fig. 4F) hours after treatment, compared to those treated with EtOH
342 for the same time. However, in the presence of EGTA, TAM-treated cells lost their ability to
343 gain self-sufficiency in growth properties, 12 (Fig. 4E) or 24 (Fig. 4F) hours after Src
344 activation. This effect is not due to cell death induced by EGTA, as EGTA-treated cells
345 survived equally well in all experimental conditions (Supp. Fig. 4C, D). EGTA does not
346 suppress the ability of TAM-treated cells to acquire sustained proliferative abilities by
347 preventing Src activation, as the phosphorylation levels of the ER-Src fusion protein (pER-Src)
348 were not significantly different between cells treated with TAM only and those co-treated with
349 TAM and EGTA (Supp. Fig. 4E).

350 We then tested if TAM-treated ER-Src cells regain a proliferative advantage after withdrawing
351 EGTA and allowing AJs re-assembly. Cells co-treated with EGTA and TAM or EtOH for 6
352 hours and left to grow in the absence of treatments for another 6 hours did not recover an

353 epithelial-like morphology with membrane-associated p120ctn at cell-cell contacts. In this
354 experimental setting, EGTA still impeded TAM-treated cells to gain proliferative competency
355 (Fig. 4G), with no effect on cell survival (Supp. Fig. 4F). However, 18 hours after withdrawing
356 EGTA and EtOH, cells completely restored an epithelial-like morphology and those that
357 received EGTA and TAM survived equally well and regained the ability to enter S-phase (Fig.
358 4H and Supp. Fig. 4G).
359 We then analyzed the impact of EGTA treatment on MRTF-A-SRF and ERK activities, as both
360 pathways provide a proliferative advantage to premalignant ER-Src cells (19,20). As previously
361 reported (20), the activity of a Luciferase reporter controlled by three SRF binding sites (SRF-
362 Luc) was significantly higher in ER-Src cells 6 hours after TAM treatment, compared to those
363 treated with EtOH. Consistent with a role of cell-cell adhesion in enabling premalignant ER-
364 Src cells to gain proliferative abilities, EGTA suppressed the transient increase in SRF-
365 dependent Luciferase activity in TAM-treated cells (Fig. 4I). EGTA also significantly
366 suppressed the higher phosphorylation levels of EGFR (pEGFR) and ERK (pERK) 12 hours
367 after TAM treatment (Fig. 4J). In these cells, ERK phosphorylation is dependent on EGFR
368 activation, as co-treating TAM-treated ER-Src cells with the EGFR inhibitor tyrphostin
369 AG1478 (EGFRi) strongly reduced pEGFR and pERK levels in both EtOH- and TAM-treated
370 cells (Supp. Fig. 4H). Taken together, these observations suggest that higher tensile forces at
371 AJs provide a proliferative advantage to premalignant ER-Src cells through the activation of
372 the EGFR-ERK and MRTF-A-SRF signaling pathways.
373
374 **P-cadherin builds up tension at AJs and FAs in premalignant ER-Src cells**
375 If higher tensile forces exerted between premalignant ER-Src cells through cadherin homophilic
376 interactions are required to strengthen tension at FAs and for cellular transformation, interfering
377 with cadherin function should phenocopy the behavior of EGTA-treated cells. MCF10A cells
378 express the two classical cadherins Ecad and Pcad (27). According to a role of Pcad-mediated
379 AJ strengthening in cellular transformation, we reported that the transient accumulation of
380 membrane-associated Pcad in premalignant ER-Src cells promotes a boost of MRTF-A-SRF
381 activity, which sustains cell proliferation (20). We therefore asked if Pcad builds up tension at
382 AJs and FAs in premalignant ER-Src cells. ER-Src cells transfected with a small interference
383 RNA against Pcad (siPcad) showed a striking decrease of membrane-associated Pcad,
384 compared to those expressing control small interference RNAs (siCTR). Yet, these cells
385 assembled in clusters with Ecad localized at the interface between neighboring cells (Fig. 5A).
386 Pcad is required to build up tension at AJs in premalignant cells, as the extended donor lifetime

of the Ecad-TS in ER-Src treated with TAM for 12 hours was significantly suppressed by expressing siPcad, compared to those expressing siCTR (Fig. 5B). Knocking down Pcad also prevented the transient extended lifetime of the Vin-TS at FAs in ER-Src cells 12 hours after TAM treatment (Fig. 5C). In contrast, reducing Pcad function in EtOH-treated cells slightly increased the donor lifetime of the Ecad-TS (Fig. 5B) and Vin-TS (Fig. 5C). We then analyzed the effect of Pcad on the activation of EGFR-ERK signaling. ER-Src cells treated with TAM for 12 hours and expressing siPcad displayed a strong reduction in Pcad, pEGFR and pERK levels, compared to those expressing siCTR (Fig. 5D).

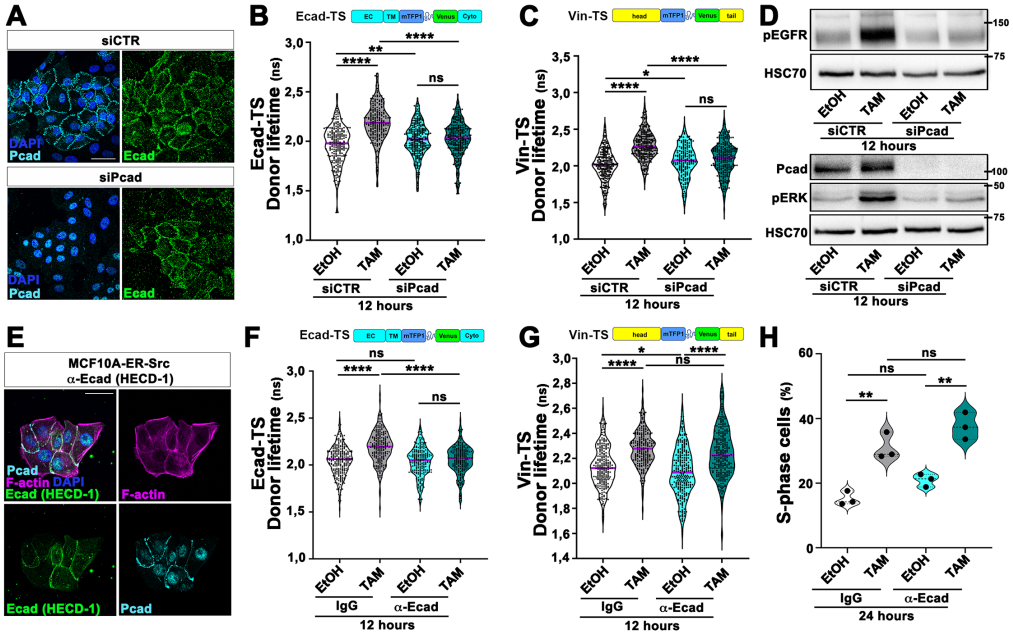

Figure 5: Pcad, but not Ecad, increases tensile forces at AJs and FAs. (A) Confocal images of ER-Src cells expressing siCTR or siPcad, stained with anti-Pcad (cyan), anti-Ecad (green) and DAPI (blue). **(B)** Quantification of the mTFP1 lifetime at AJs in ER-Src cells expressing the Ecad-TS and siCTR or siPcad and treated with EtOH or TAM for 12 hours. **(C)** Quantification of the mTFP1 lifetime at FAs in ER-Src cells expressing the Vin-TS and siCTR or siPcad and treated with EtOH or TAM for 12 hours. **(D)** Western blots on protein extracts from ER-Src cells expressing siCTR or siPcad and treated with EtOH or TAM for 12 hours, blotted with anti-pEGFR and anti-HSC70 used as loading control or anti-Pcad, anti-pERK and anti-HSC70. **(E)** Confocal images of ER-Src cells incubated with 10 µg/mL of the Ecad blocking antibody HECD-1 (green), stained with Phalloidin (magenta), anti-Pcad (cyan) and DAPI (blue). **(F)** Quantification of the mTFP1 lifetime at AJs in ER-Src cells expressing the Ecad-TS and treated with EtOH or TAM in the presence of IgG or Ecad blocking antibody for 12 hours. **(G)** Quantification of the mTFP1 lifetime at FAs in ER-Src cells expressing the Vin-TS and treated with EtOH or TAM in the presence of IgG or Ecad blocking antibody for 12 hours. **(H)** Quantifications of the percentage of ER-Src cells in S-phase treated with EtOH or TAM for 24 hours in the presence of IgG or anti-Ecad blocking antibody. Quantifications are from three biological replicates and are presented as violin plots with the magenta lines indicating median values. Statistical significance was calculated using one-way ANOVA with Tukey's multiple comparison. ns indicate non-significant. *P<0,05; **P<0.01; ***P<0.001; ****P<0.0001. Scale bar indicates 20 µM.

416

417 We then tested the role of Ecad in increasing tensile forces at FAs and in cellular transformation.
418 Unlike Pcad, the levels of the mature and pro-peptide Ecad forms were not significantly
419 different between cells treated with EtOH and TAM for 12 hours (Supp. Fig, 5). To analyze the
420 consequence of affecting Ecad function on FA strengthening, we blocked the *trans* junctional
421 homophilic interactions between the Ecad extracellular domains using the Ecad blocking
422 antibody HECD-1. As expected, HECD-1 was found associated with the cell membrane. These
423 cells were still assembled in clusters with Pcad localized at the interface between neighboring
424 cells (Fig. 5E). Although the Ecad blocking antibody prevented the extended donor lifetime of
425 the Ecad-TS in cells treated with TAM for 12 hours (Fig. 5F), it did not suppress the higher
426 Vin-TS donor lifetime in these cells (Fig. 5G), nor their ability to enter S-phase (Fig. 5H). Taken
427 together, we conclude that higher tensile forces at AJs, exerted between TAM-treated ER-Src
428 cells through Pcad homophilic interactions, is required for building up tension at FAs and for
429 ERK-dependent proliferation.

430

431 **Cadherin is required for Src-induced overgrowth *in vivo***

432 We then tested if AJs were required for Src-induced overgrowth *in vivo*. *Drosophila* Ecad
433 (DEcad), encoded by *shotgun*, is the main classical cadherin contributing to cell-cell adhesions
434 in the wing disc epithelium (28). We therefore tested if knocking down *DEcad* suppresses the
435 overgrowth of *Drosophila* wing discs overexpressing the *Src oncogene at 64B (Src64B)* and
436 the caspase inhibitor *p35* using the UAS-Gal4 system. As expected, distal wing discs
437 overexpressing *Src64B, p35* and two copies of Green Fluorescent Protein (GFP) with the
438 *nubbin*-Gal4 (*nub*-Gal4) driver were bigger than control discs expressing GFP only. Strikingly,
439 replacing one copy of UAS-GFP by a UAS construct expressing double-strand RNA (dsRNA)
440 directed against *Ecad (DEcad-IR#1)* appeared to reduce the growth of *Src/p35*-expressing wing
441 discs (Fig. 6A). Quantification of the ratio between the GFP-positive area and the total wing
442 area for each experimental condition confirmed that knocking down *DEcad* significantly
443 suppressed the overgrowth of *Src/p35*-expressing wing discs (Fig. 6A). Expressing an
444 independent dsRNA against *DEcad (DEcad-IR#2)* also significantly suppressed the overgrowth
445 of *Src64B/p35*-expressing wing discs (Fig. 6B). To confirm that the overgrowth suppression
446 observed reflected indeed a reduction in cell number, we also evaluated the percentage of GFP-
447 positive cells by cell sorting for each experimental condition. While the number of GFP-positive
448 cells was significantly increased by 22% in *nub>Src64B, p35*-expressing wing discs, compared
449 to control discs expressing *GFP* only, knocking down *DEcad* in these tissues restored the

percentage of GFP-positive cells to those of control discs expressing *GFP* only (Fig. 6C and Supp. Fig. 6). These observations are in agreement with a role for AJs in Src-induced tissue growth.

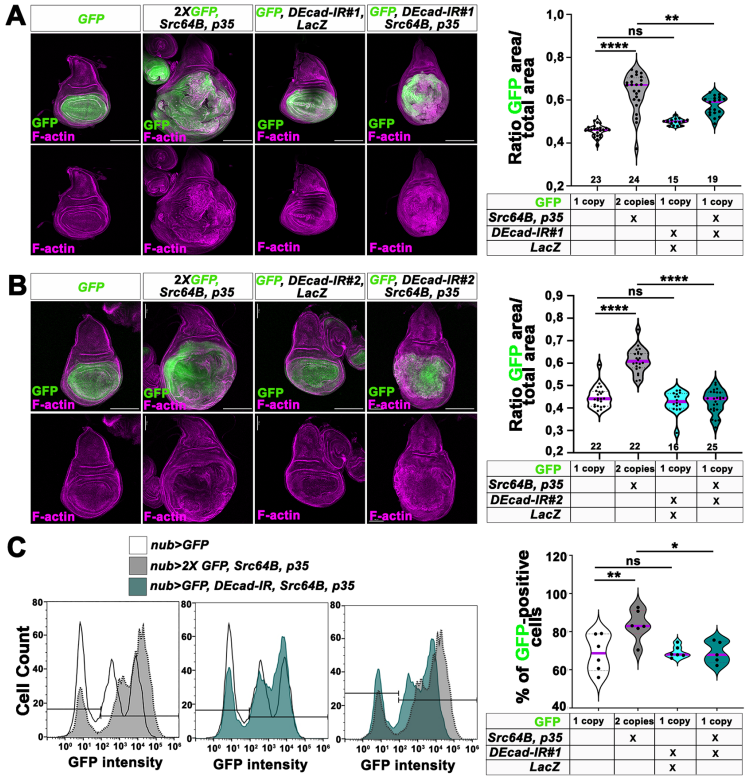

Figure 6: Knocking down *DEcad* suppresses the overgrowth induced by Src overexpression *in vivo*. (A) (Left) Standard confocal sections of third instar wing imaginal discs with dorsal side up, expressing one copy of UAS-CD8::GFP (green) or two copies of UAS-*CD8::GFP* (green), UAS-*p35* and *Src64B*^{UY1332} or one copy of UAS-*CD8::GFP* (green), UAS-*LacZ* and UAS-*DEcad-IR*^{GL00646} or one copy of UAS-*CD8::GFP* (green), UAS- *DEcad-IR*^{GL00646}, UAS-*p35* and *Src64B*^{UY1332} under *nub*-Gal4 control. Discs are stained with Phalloidin (magenta). (Right) Ratio of the *nub>GFP* area over the total wing disc area for the genotypes indicated. Number of samples analyzed are indicated on the X axis, and are from two biological replicates. **(B)** (Left) Standard confocal sections of third instar wing imaginal discs with dorsal side up, expressing one copy of UAS-CD8::GFP (green) or two copies of UAS-*CD8::GFP* (green), UAS-*p35* and *Src64B*^{UY1332} or one copy of UAS-*CD8::GFP* (green), UAS-*LacZ* and UAS-*DEcad-IR*^{GD14421} or one copy of UAS-*CD8::GFP* (green), UAS- *DEcad-IR*^{GD14421}, UAS-*p35* and *Src64B*^{UY1332} under *nub*-Gal4 control. Discs are stained with Phalloidin (magenta). (Right) Ratio of the *nub>GFP* area over the total wing disc area for the genotypes indicated. Number of samples indicated on the X axis are from three biological replicates. **(C)** (Left) Histograms of membrane-associated GFP levels in wing discs from the genotypes indicated. (Right) Percentage of GFP-positive cells in wing discs from the genotypes indicated. Quantifications are from five biological replicates. Quantifications are presented as violin plots with the magenta lines indicating median values. Statistical significance was calculated using one-way ANOVA with Tukey's multiple comparison. ns indicate non-significant. **P<0.01; ***P<0.001; ****P<0.0001. Scale bar indicates 20 µM.

476 **Discussion**

477 The weakening of cell-cell and cell-matrix adhesiveness has been proposed to allow cancer
478 cells to acquire hallmarks of malignant tumors, including sustaining proliferative signaling,
479 resisting cell death and activating invasion and metastasis (29). Here, we provide evidence that
480 AJs and FAs have a paradoxical role in premalignant breast epithelial cells overactivating Src.
481 We show that prior to undergoing EMT, a transient mechanical crosstalk between Pcad-
482 mediated forces transmission at AJs and FAs provide a proliferative advantage to ER-Src cells
483 through activation of the EGFR-ERK and MRTF-A-SRF signaling (Fig. 7).

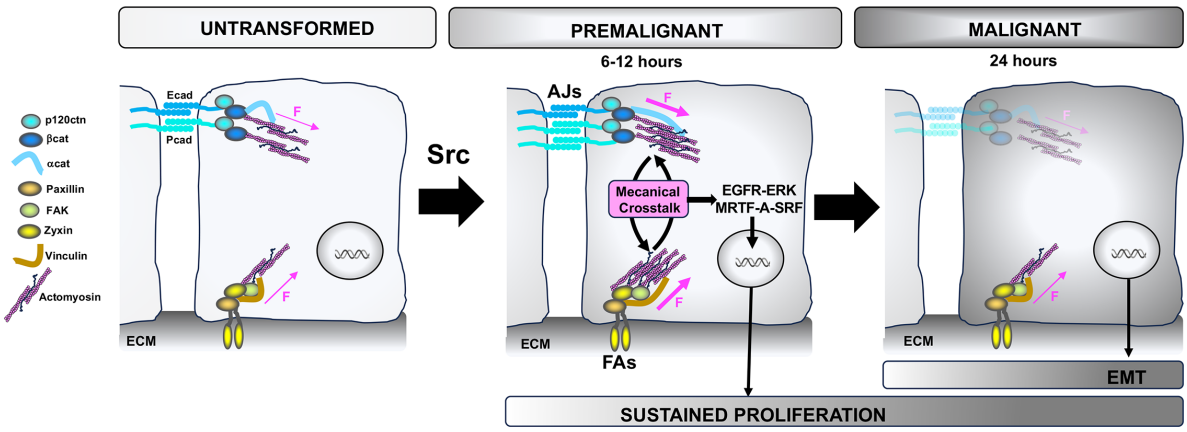

484

485 **Figure 7: Model by which the transient mechanical crosstalk between AJs and FAs in**
486 **premalignant ER-Src cells sustains cell proliferation, prior to undergoing EMT.**
487 Premalignant Src-overactivating MCF10A cells accumulate membrane-associated Pcad, which
488 increases tensile forces at AJs and FAs. In turn, FAs transmit tensile forces to AJs. This positive
489 mechanical crosstalk triggers activation of the EGFR-ERK and MRTF-A-SRF signaling
490 pathways, which provide to TAM-treated ER-Src cells a proliferative advantage. Later, cells
491 lose membrane-associated Ecad and Pcad, reduce tensile forces at FAs and acquire features
492 associated with EMT.

493

494 Our observations demonstrate that prior to triggering features associated with EMT, Src
495 transiently buildups tension at AJs and FAs that are transferred between both adhesion sites.
496 During the first 12 hours of Src activation, Ecad and αcat at AJs and Vinculin at FAs bear
497 higher forces that correlate with the assembly of larger FAs. Moreover, premalignant cells
498 unable to assemble AJs due EGTA or that fail to strengthen tension at AJs due to Pcad
499 depletion, lose the ability to reinforce tension at FAs. Conversely, preventing the strengthening
500 of tensile forces at FAs by restricting FAK or Paxillin activity, suppresses the ability of
501 premalignant ER-Src cells to build up higher tensile forces at AJs. The requirement for
502 increased tensile forces at AJs prior to EMT may not be unique to MCF10A cells with
503 conditional Src activation. In the *Drosophila* wing disc epithelium, tension at AJs is required

504 in pre-tumoral tissues for subsequent tumor evolution (30). Likewise, Hepatocyte Growth
505 Factor (HGF) enhances homophilic Ecad interaction in MDCK cells prior to inducing AJ
506 disassembly (31). EGF also increases the magnitude of tensile force on Ecad in MCF10A cells
507 prior to triggering cell scattering (32). Thus, major alterations in AJs and FAs could constitute
508 prime events in cancer development, ahead of any signs of EMT. Consistent with this
509 possibility, we reported that the two most significant pathways affected in premalignant breast
510 atypical hyperplasia are components of the AJ and FA adhesomes (19).
511
512 We propose that higher tensile stresses at AJs provide a proliferative advantage to Src-
513 overactivating cells by promoting activation of the EGFR-ERK and MRTF-A-SRF signaling
514 pathways. Consistent with this model, TAM-treated ER-Src cells unable to assemble AJs due
515 to EGTA, lose the ability to gain a proliferative advantage and to enhance EGFR-ERK and
516 MRTF-A-SRF signaling activities. In turn, ERK and MRTF-A are required to sustain
517 proliferation in those cells (19,20). Moreover, TAM-treated cells regain self-sufficiency in
518 growth capacity if empowered to re-assemble AJs. Furthermore, *in vivo*, DEcad, the sole
519 classical cadherin involved in AJ-dependent cell-cell adhesions, enables the overgrowth of Src-
520 overexpressing wing discs. In agreement with our observations, Myosin II activity is required
521 for ERK-mediated proliferation in premalignant ER-Src cells (19). Mechanical stresses can
522 also activate EGFR-ERK and trigger MRTF-A nuclear translocation in other cell models
523 (33,34). Ligand-independent ERK activation can be induced by Ecad extracellular
524 engagement, which phosphorylates EGFR at cell-cell contact in keratinocytes (35).
525 Premalignant ER-Src cells do not require Ecad trans-homophilic interaction to enter S-phase.
526 Rather, this function is endorsed by Pcad, which transiently accumulates at the cell membrane
527 and triggers a boost of MRTF-A-SRF signaling activity (20). In addition, we show that Pcad
528 is required to potentiate EGFR-ERK activity in premalignant cells. Pcad also triggers EGFR
529 signaling in oral dysplastic keratinocytes (36). Moreover, in premalignant ER-Src cells, Pcad
530 is necessary to increase tensile forces on Ecad at AJs. Consistent with our observations, Pcad
531 mediates intercellular force transmission in MCF10A cells (37). However, in breast cancer cell
532 lines, Pcad reduces tension at AJs and destabilizes the interaction between Ecad and catenins
533 (38,39). Pcad overexpression is also strongly associated with cytoplasmic p120ctn
534 accumulation in pancreatic and ovarian cancer cell lines (40,41). Thus, Pcad may have a dual
535 opposite effect on AJ strengths that could depend on the stage of tumor progression and
536 therefore on the composition of the AJ adhesomes. Yet, the mechanism by which the Pcad-

537 dependent force transmission activates the EGFR-ERK and MRTF-A-SRF signaling pathways
538 remains to be characterized.
539
540 In addition, to provide a proliferative advantage to premalignant ER-Src cells, EGFR activation
541 mediated by force transmission at AJs may also build up tensile stresses at FAs. In agreement
542 with this model, EGFR activation increases tension on integrin and controls the spatial
543 organization of FAs in Cos-7 cells (42). Likewise, in MCF7 cells, EGFR activation increases
544 FAs size and number and integrin-mediated traction forces (17). Yet, we cannot exclude that
545 Pcad-mediated force transmission affects EGFR-ERK- and MRTF-A-SRF activities through
546 increasing tensile forces at FAs. EGFR has also been shown to interact with integrin in human
547 fibroblasts and endothelial cells and is activated by integrin-mediated adhesions even in the
548 absence of EGF, leading to ERK activation (43). In turn, EGFR signaling can reinforce AJs
549 and junctional actomyosin, as shown in the *Drosophila* ectoderm prior to gastrulation onset
550 (44). Integrin-mediated force transmission can also trigger MRTF-A nuclear translocation (45).
551 Moreover, we show that FAK and Paxillin are required for force transmission at FAs in
552 premalignant ER-Src cells, as well as for sustaining cell proliferation. However, as FAK and
553 Paxillin also strengthen tension at AJs, the growth defect of Src-overactivating ER-Src cells
554 defective for FAK or Paxillin activity could result from the shortfall in AJ strengthening.
555 Forces transmitted from FAs to AJs could further increase tensile forces at AJs, which, upon
556 reaching a certain threshold may trigger the subsequent dissociation of F-actin from AJs and
557 the loss of cell-cell adhesions required for EMT, as proposed in endothelial cells (46). Thus,
558 while uncontrolled growth because of the loss of cell-cell contacts has been proposed to enable
559 the initiation and progression of several types of cancer (47), our work reveals that a transient
560 mechanical crosstalk between AJs and FAs in premalignant breast cells could drive tumor
561 growth.

562 **Methods**

563

564 ***Fly strains and genetics.***

565 Fly stocks used were UAS- *DEcad-IR*^{GD14421} (Vienna Drosophila Research Center, VDRC),
566 and *nub*-Gal4, Src64B^{UY1332}, UAS-*p35*, UAS-*DEcad-IR*^{GL00646} (Bloomington Drosophila
567 Stock Center). All crosses were maintained at 25 ºC. Male and female larvae were dissected at
568 the end of the third instar.

569

570 ***Cell culture conditions and treatments***

571 The MCF10A-ER-Src cell line (ER-Src for short), kindly provided by K. Struhl (48), was
572 grown in Complete Growth Media (CGM), composed of DMEM/F12 growth media (Gibco,
573 11039-047), supplemented with 5% of Charcoal Stripped Horse Serum (CSHS) (Gibco, 16050-
574 122), 20 ng/mL human EGF (Peprotech, AF-100-15), 0.5 µg/mL Hydrocortisone (Sigma,
575 H0888), 100 ng/mL Cholera toxin from Vibrio cholerae (Sigma, C8052), 10 µg/mL Insulin
576 (Sigma, I9278), 0.5 µg/mL Puromycin (Merck, 540411) and 1% Penicilin-Streptomycin
577 (Gibco, 15140). To treat cells with 1 µM 4OH-TAM (Merck, H7904) or EtOH, cells were
578 plated in CGM at 50% confluency and allowed to adhere for 12 to 24 hours. Cells were then
579 treated with 1 µM 4OH-TAM (Merck, H7904) or an equal volume of EtOH for the time
580 indicated

581 To analyze the effect of EGTA, cells were plated in CGM at 50% confluency, allowed to adhere
582 for 12 to 24 hours and starved in Restricted Growth Media (RGM), composed of DMEM/F12,
583 supplemented with 0.5% CSHS, 20 ng/mL human EGF, 0.5 µg/mL hydrocortisone, 100 ng/mL
584 cholera toxin, 10 µg/mL insulin, 0.5 µg/mL Puromycin and 1% Penicillin-Streptomycin for 12
585 hours. Cells were then treated with 4 mM EGTA (BioWorld, 40520008) or left without
586 treatment for 30 minutes, and co-treated with 1 µM 4OH-TAM or an equal volume of EtOH
587 for the indicated time. For cell cycle analysis, RGM media without EGF was used.

588 To block the *trans* junctional homophilic interactions between Ecad extracellular domain, cells
589 were seeded and allowed to adhere in the presence of 10 µg/mL of anti-Ecad monoclonal
590 antibody (HECD-1, Invitrogen, 13-1700) or with an identical volume of IgG in CGM. Cells
591 were then starved for 12 hours in RGM lacking EGF in the presence of HECD-1 or IgG and
592 co-treated with 1 µM 4OH-TAM or EtOH and HECD-1 or IgG for 24 hours for cell cycle
593 analysis or directly co-treated with 1 µM 4OH-TAM or EtOH and HECD-1 or IgG in CGM
594 for all other experiments for the time indicated.

595 To inhibit FAK activity, cells were plated in CGM and allowed to adhere for 24 hours. Cells
596 were then treated with 8 μM PF-573228 (Sigma-Aldrich, PZ0117) or DMSO for 12 hours in
597 RGM lacking EGF for cell cycle analysis or for 2 hours in CGM for all other experiments.
598 Cells were then co-treated with EtOH or 1 μM 4OH-TAM and PF-573228 or DMSO for the
599 indicated time in RGM lacking EGF for cell cycle analysis or CGM for all other experiments.
600 To inhibit EGFR activity, cells were seeded in CGM and allowed to adhere for 24 hours. Then,
601 cells were washed twice, grown in DMEM/F12 for 12 hours, and treated with 2 μM of the
602 EGFR inhibitor for 1 hour, and co-treated with 1 μM 4OH-TAM or EtOH in the presence or
603 absence of 2 μM AG1478 (Santa Cruz Biotechnology, sc-200613) for the indicated time.
604 The Human Embryonic Kidney 293T cells (HEK293T) used for viral production were grown
605 in DMEM/F12 supplemented with 10% Fetal Bovine Serum (FBS) Premium heat-inactivated
606 (Thermo Fisher Scientific, 10500-064). MDA-MB-231 cells were grown in Dulbecco's
607 Modified Eagle Medium (DMEM) High Glucose 1X + GlutaMAX™-I (Thermo Fisher
608 Scientific, 31966), supplemented with 10% FBS and 1% Penicillin-Streptomycin (Thermo
609 Fisher Scientific, 15070-063).
610 All cell lines were grown in a humidified incubator at 37 °C, under a 5% CO_2 atmosphere.
611 Tests for mycoplasma contamination were performed every other month, via PCR using the
612 primers MGS0 5′-TGCACCATGTGTCACTCTGTTAACCTC-3′ and GPO1 5′-
613 ACTCCTACGGGAGGCAGCAGTA-3′, which amplify the 16S ribosomal RNA genes of the
614 Mollicutes class of mycoplasma.
615
616 ***Molecular Biology***
617 Ecad-TS and Ecad-TSΔCyto constructs were generated from the canine EcadTSMod sequence
618 kindly provided by Alex Dunn lab (Stanford University) (10). Briefly, the cassette containing
619 the Ecad-TS or Ecad-TSΔCyto was excised with EcoRI and XbaI, and inserted within the
620 pGenLenti vector. Vin-TS and Vin-TSΔtail constructs were generated from the Addgene
621 plasmids #26019 and #26020, kindly provided by Martin Schwartz (9). Both plasmids were
622 excised from their backbone using the HindIII and SacII restriction enzymes and inserted into
623 the pGenLenti vector.
624
625 ***Lentivirus production and infection***
626 To produce shLuc (Sigma Aldrich, TRCN0000123137), shPXN (Sigma Aldrich,
627 TRCN0000123137), Ecad-TS, Ecad-TSΔcyto, Vin-TS, or Vin-TSΔtail viral particles,
628 HEK293T cells were seeded to reach 70-80% confluency and transfected with 6 μg of pMD2.G

629 (envelope vector), 17 µg of psPAX2 (packaging vector), and 22 µg of plasmids of interest using
630 Lipofectamine 2000 (Thermo Scientific, 11668019). Supernatants were collected 48 and 72
631 hours after transfection, centrifuged at 500 g for 10 minutes, and filtered using a 0.45 µm filter
632 unit to remove large cellular debris, followed by concentration through ultracentrifugation
633 using the Optima L-80 XP Ultracentrifuge (Beckman Coulter) at 32,000 *g* for 1.5 hours at 4ºC.
634 Pellets were resuspended in CGM, aliquoted, and stored at -80ºC. To infect ER-Src cells, plated
635 in 6-well plates, CGM was replaced with 1 mL of CGM supplemented with 10 µg/mL
636 Polybrene® (EMD Millipore, TR-1003-G). Lentiviral particles were added dropwise to each
637 well and mixed by gentle swirling. 12h later, 1 mL of CGM media was added to each well.
638 Cells were incubated for 72 hours and assessed for protein expression by flow cytometry or
639 western blot.
640
641 ***FRET-FLIM Analysis***
642 To perform FRET-FLIM experiments, ER-Src cells stably expressing each FRET-based sensor
643 (Ecad-TS, Ecad-TSΔCyto, Vin-TS, Vin-TSΔtail) were plated on an ibiTreat 8-well chamber
644 slide (Ibidi, 80826) in CGM and allowed to adhere for 24h. After treatment, images were
645 acquired on a single point scanning confocal Stellaris 8, equipped with a fully motorized
646 inverted Leica DMI8 microscope, an HC PL APO 86x/1.20 W motCORR STED white water
647 immersion objective equipped with a correction collar (Leica Microsystems), a WLL, and
648 Falcon and STED modalities, using the Leica LASX software (version 4.6.1.27508). Cells
649 were selected using the acceptor fluorescence signal (EYFP) to ensure the proper localization
650 of the tension sensor (AJs for Ecad-TS and FAs for Vin-TS). The Navigator function on LASX
651 was used to have an overview of the sample and to identify clusters of cells. Fluorescent
652 proteins were excited using a white light laser (WLL) at 85% power, tuned to 80 MHz. The
653 WLL was tuned to 440 or 514 nm to excite mTFP1 and EYFP, respectively, with laser powers
654 of 2% and 2%. Photon detection was performed using two Power HyD X detectors in photon
655 counting (intensity mode), tuned to 440 nm (mTFP1). Images were recorded sequentially by
656 frame scanning unidirectionally at 400 Hz using the galvanometer-based imaging mode, with
657 a line accumulation of 16, and a pixel size of 0.176 µm for an area size of 20,83 µm x 20,83
658 µm (512 x 512, zoom factor of 1, pixel dwell time of 3.1625 µs). For each experiment, a
659 minimum of 20 cell clusters were analyzed.
660 FRET detection was based on the time-domain FLIM experiments, which were performed
661 using time-correlated single-photon counting. At least 100 photon events per pixel were

662 collected in all cases, and the lifetime analysis was performed using the Phasor approach on
663 LASX.
664
665 ***Immunofluorescence Analysis***
666 Wing imaginal discs from third instar larvae were dissected in a phosphate buffer at pH 7 (0.1
667 M Na2HPO4, 0.1 M NaH2PO4 at a 72:28 ratio). Discs were then fixed in 4 % formaldehyde
668 in PEM (0.1 M PIPES pH 7, 0.2 mM MgSO4, 1 mM EGTA) for 20 to 30 min, rinsed in
669 phosphate buffer 0.2 % Triton for 15 minutes and incubated 2 hours at 4ºC with Rhodamine-
670 conjugated Phalloidin (Sigma, P-1951) at 0,3 mM in phosphate buffer 0.2 % Triton
671 supplemented with 10 % horse serum. Wing discs were washed 3 times, 10 minutes each,
672 before being mounted in Vectashield (Vector Labs, H-1000). Fluorescence images were
673 acquired on a single point scanning confocal SP5, equipped with a fully motorized inverted
674 Leica DMI6000 microscope, an HC PL APO Lbl. Blue 20x/0.70 IMM objective equipped with
675 a correction collar (Leica Microsystems).
676 For cells, $1.5x10^5$ ER-Src or $1x10^5$ E-cad TS, Vinc-TS, Ecad-TSΔcyt, Vin-TSΔtail cells were
677 seeded on poly-L-lysine-coated coverslips and allowed to adhere for 12 to 24 hours. After
678 treatment, cells were rinsed with PBS 1X and fixed with 4% formaldehyde methanol-free
679 (Thermo Fisher Scientific, 28908) in H_2O, supplemented with 0.06 M PIPES pH 6.8, 0.03 M
680 HEPES pH 7.0, 0.01 M EGTA pH 6.8, and 0.004 M $MgSO_4$ for 10 minutes. Cells were
681 permeabilized with PBS containing 0.1% Triton-X-100 (PBS-T) for 2 minutes at RT and
682 blocked with a blocking buffer (10% FBS in PBS-T) for 1 hour at RT. Rat anti-α18 (1:50; a
683 gift from Professor Akira Nafaguchi, Japan, (23), mouse anti-p120ctn (1:50; BD Bioscience,
684 610133), rabbit anti-Zyxin (1:50; Sigma, HPA004835), mouse anti-Ecad (1:50; Invitrogen, 13-
685 1700), mouse anti-Pcad (1:50; BD Bioscience, 610228), rabbit anti-Ecad (1:50; Cell
686 Signalling, 3195) and mouse anti-Paxillin (1:50 or 1:200; BD Bioscience, 610051) were
687 incubated overnight at 4ºC in blocking buffer. Coverslips were washed with PBS 1X three
688 times for 5 minutes at RT and incubated with FITC-conjugated Donkey anti-Rat IgG (1:200;
689 Jackson ImmunoResearch, 712-095-150), FITC-conjugated Donkey anti-Mouse IgG (1:200;
690 Jackson ImmunoResearch, 715-095-150), Alexa Fluor 647-conjugated Donkey anti-Mouse
691 IgG (1:200; Jackson ImmunoResearch, 715-605-151), CyTM5-conjugated Donkey anti-Rabbit
692 IgG (1:200; Jackson ImmunoResearch, 711-175-152), and Rhodamine-conjugated Phalloidin
693 (Sigma-Aldrich, P-1951) at 0.3 mM in blocking buffer for 1 hour at RT in the dark. After three
694 washes with PBS 1X for 5 minutes, cells were stained with DAPI (1:500; Sigma, D9542) for
695 5 minutes at RT, washed with PBS 1X for 5 minutes, and mounted in Vectashield. Images were

696 obtained on a single-point scanning confocal Leica SP5, coupled to a Leica DMI6000, using
697 the 63x/1.4 HCX PL APO CS oil immersion objective or with a spinning disk confocal Andor
698 BC43 benchtop system (Oxford Instruments/Andor) using the 60x/1.42 oil immersion
699 objective. Image processing was performed using Imaris version 10.2 or NIH Fiji/ImageJ.
700
701 ***Immunoblotting Analysis and Quantification***
702 $2.65x10^5$ ER-Src cells in CGM were plated in a T25 flask. After 6 or 12 hours of treatment,
703 cells were trypsinized with TrypLE™ Express (Gibco, 12604-021) and collected into 1.5 mL
704 tubes. Proteins were extracted by resuspending the cell pellets in Lysis Buffer SDS-Free,
705 composed of 0.05M Tris-HCl pH 7.5 (VWR, 33621.260), 0.15 M NaCl (Sigma-Aldrich,
706 31434), 0.001 M EDTA pH 8.0 (Sigma-Aldrich, E5134), 0.001 M EGTA pH 7.0 (Sigma-
707 Aldrich, E3889), 1% Triton X-100 (Sigma-Aldrich, T8787) and supplemented with 1%
708 protease inhibitors (Sigma-Aldrich, 5892791001) and 1% phosphatase inhibitors (Sigma-
709 Aldrich, 4906845001) on ice for 30 minutes. Samples were centrifuged at 4°C for 30 minutes
710 at 14,000 rpm, and protein was quantified using the Bradford method. For pERK and pEGFR
711 detection, $1.5x10^5$ ER-Src cells were plated in 6-well plates. After 12 hours of treatment, Lysis
712 Buffer SDS-Free, containing 1% protease inhibitors (Sigma-Aldrich, 5892791001) and 1%
713 phosphatase inhibitors (Sigma-Aldrich, 4906845001; Sigma-Aldrich, S6508; Sigma-Aldrich,
714 S7920), was added to cells. Cells were detached using a cell scraper and collected into 1.5 mL
715 tubes. Samples were centrifuged at 4°C for 30 minutes at 14,000 rpm, and protein was
716 quantified using the Bradford method. Laemmli buffer was added to protein samples to a final
717 concentration of 1X, and extracts were boiled for 5 minutes at 95°C, centrifuged for 10 minutes
718 at 8,000 rpm before being resolved by SDS-PAGE electrophoresis and transferred to a 0.45
719 μM PVDF blotting membrane (Amersham, 10600023). Membranes were blocked with 5%
720 BSA in TBS containing 0.1% Tween 20 for 1 hour, cut to separate proteins migrating at diverse
721 molecular weights and incubated with rat anti-α18 (1:1,000; (Nagafuchi & Tsukita, 1994)),
722 rabbit anti-αcat (1:1,000; Thermo Fisher Scientific, MA5-14986), mouse anti-HSC70 (1:8,000;
723 Santa Cruz Biotechnology, sc-7298), mouse anti-Paxillin (1:10,000; BD Bioscience, 610051),
724 mouse anti-phospho-p44/42 MAPK (1:1,000; Cell Signaling, 9106), rabbit anti-p44/42 MAPK
725 (1:2,000; Cell Signaling, 9102), rabbit anti-GAPDH (1:5,000; Sigma, G9545), rabbit anti-
726 pEGFR (1:1,000; Thermo Fisher Scientific, 44-788G) mouse anti-Pcad (1:2,500; BD
727 Bioscience, 610228), rabbit anti-pFAK (pY397) (1:1,000; Cell Signalling), rabbit anti-Ecad
728 (1:1,000; Cell Signalling, 3195) and rabbit anti-phospho Src (pY418) (1:3,000; Invitrogen, 44-
729 660G) diluted in TBS 0.1% Tween 20 supplemented with 3% BSA. Secondary antibodies used

730 were horseradish peroxidase (HRP)-conjugated AffiniPure donkey anti-mouse IgG (1:5,000;
731 Jackson ImmunoResearch, 715-035-150), HRP-conjugated AffiniPure donkey anti-rabbit IgG
732 (1:5,000; Jackson ImmunoResearch, 715-035-152), goat anti-rat IgG-HRP (1:5,000; Santa
733 Cruz biotechnology, sc-2006), IRDye® 680RD-conjugated donkey anti-mouse IgG (1:20,000;
734 LI-COR Bioscences, 926-68072) and IRDye® 800CW-conjugated donkey anti rabbit IgG
735 (1:20,000; LI-COR Bioscences, 926-32213), all diluted in TBS 0.1% Tween 20 supplemented
736 with 1% BSA. Immobilon Western Chemiluminescent HRP substrate (Millipore, P90719) was
737 utilized for detection and visualization in ChemiDoc (Bio-Rad) or Odyssey® M (LI-COR
738 Biosciences) imaging systems. Image Lab (Bio-Rad) and Image Studio (LICOR) software were
739 used for quantification. The intensity levels of each band were normalized to those of the
740 respective control for protein extracts loaded on the same gel for each experimental condition.
741
742 ***Transfections and dual Luciferase Renilla reporter assay***
743 To test the effect of knocking down Pcad, $1.5x10^5$ ER-Src cells resuspended in 2 mL of CGM
744 were plated in 6-well plates for immunoblot analysis or in ibiTreat 8-well chamber slide for
745 FRET-FLIM analysis. After 12 to 24 hours, cells were transfected with 50 nM or 100nM siCTR
746 (Qiagen, 1027310) or 50 nM or 100nM siCDH3 (Qiagen, 1027416, GeneGlobe
747 ID:SI02663941) for FRET-FLIM and immunofluorescence or for immunoblot analysis,
748 respectively, using Lipofectamine 2000, according to the manufacturer's instructions. After 24
749 hours, transfected cells were incubated for another 12 hours in CGM containing EtOH or 4OH-
750 TAM for FRET-FLIM or immunofluorescence analysis. For immunoblot analysis, 12 hours
751 after transfection, the medium was replaced by RGM lacking EGF. After 36 hours, cells were
752 treated with 4OH-TAM or EtOH for the indicated time. To test the effect of EGTA on the
753 activity of the SRF-Luc reporter, $1x10^5$ cells resuspended in 2 mL of CGM were plated in 6-
754 well plates. 12 to 24 hours later, cells were transfected with 0.720µg p3D.A-Luc and 1.44 µg
755 pRL-TK plasmids (49) using Lipofectamine 2000, according to the manufacturer's
756 instructions. Cells were then incubated with EGTA for 30 minutes, and co-treated with 4OH-
757 TAM or EtOH in the presence or absence of EGTA for 6 hours in RGM lacking EGF. After
758 trypsinization with TrypLE™ Express (Thermo Fisher Scientific, 12604021), cell pellets were
759 resuspended in 250 µL 1× passive lysis buffer (Promega, E1941) and stored overnight at
760 −20°C. Luciferase assay was performed using a Dual-Luciferase Reporter Assay system
761 (Promega, PROME19600010) according to the manufacturer's instructions. Briefly, 100 µL
762 Luciferase assay reagent II (LARII) was added to 80 µL of lysed samples in a 96-well plate.
763 Firefly luminescence was detected using Synergy Mx (BioTek). Then, 100 µL 1X Stop and

764 Glo solution (Promega, PROME19600010) was added to detect Renilla luminescence. Each
765 sample was evaluated in triplicate.
766
767 ***Cell Cycle Profile***
768 For cell cycle analysis, cells treated for 12 or 24 hours were trypsinized with TrypLE^{TM} Express
769 and collected into 5 mL round-bottom polystyrene tubes (Corning, 352235). Cells were
770 centrifuged for 5 minutes at 1,000 rpm at 4ºC, washed with 1 mL of FACS Buffer (PBS 1X
771 supplemented with 2% heat-inactivated FBS (Biowest, S181BH)), centrifuged for 5 minutes at
772 1,000 rpm at 4ºC and resuspended in 500 µL FACS Buffer. Cells were fixed with 1.5 mL 70
773 % Ethanol, added drop-by-drop, while gently vortexed, followed by a 30 minutes incubation
774 at 4ºC. After 5 minutes centrifugation at 2,000 rpm at 4ºC, cells were resuspended in 3 mL of
775 ice-cold PBS 1X, incubated 30 minutes on ice, pelleted again by centrifugation for 5 minutes
776 at 2,000 rpm at 4ºC and resuspended in 300 µL of PBS 1X, supplemented with 100 µg/mL
777 RNAse A (Qiagen, 19101) and 20 µg/mL Propidium Iodide (Sigma, P4170). Samples were
778 incubated for 30 minutes in a 37ºC water bath in the dark. Flow Cytometry was performed at
779 a low flow rate using a BD Accuri C6 Flow Cytometer (Becton-Dickinson, Franklin Lakes,
780 NJ, USA). Cell Cycle profiles were analyzed using FlowJo 10.7.1 software (Tree Star, Inc.,
781 Ashland, OR, USA) Cell Cycle platform, using the Watson Model.
782
783 ***Quantification of cell number***
784 To quantify cell number, cells were trypsinized with TrypLE^{TM} Express, washed twice with
785 PBS 1X, and resuspended in PBS 1X. Then, cell suspension was mixed with trypan blue in a
786 1:1 proportion, pipetted into a disposable Countess cell counting chamber slide (Thermo Fisher
787 Scientific, C10228) and cell number was quantified using the Countess 3 Automated Cell
788 Counter (Thermo Fisher Scientific).
789
790 ***Flow Cytometry***
791 To quantify GFP-expressing cells in wing imaginal discs, 25 discs were dissected for each
792 genotype in ice-cold PBS 1X. Samples were then incubated in 200 µL of TrypLE™ for 45
793 minutes at 37°C to facilitate cell dissociation. Mechanical pipetting was performed to ensure
794 complete dissociation before inactivating the TrypLE™ with 200 µL of PBS 1X supplemented
795 with 1% FBS. Cells were centrifuged at 3,500 rpm for 8 minutes, fixed in 500 µL of ice-cold
796 70 % Ethanol, and stored at 4°C. Before analysis, cells were resuspended in 400 µL of PBS
797 1X, and filtered into 5 mL FACS round-bottom tubes. 100 µL of cell suspension was analyzed

798 with medium flow rate settings on a BD Accuri C6 Plus. A description of the gating strategy
799 can be found in Supp. Fig. 6. To confirm the expression of the FRET-tension sensors,
800 transduced ER-Src cells were washed and resuspended in PBS 1X supplemented with 0.2%
801 BSA and 0.1% NaN3, at a concentration of $1x10^6$ cells/ml. Cytometric analysis was performed
802 using a FACSCanto II or LSRFortessa flow cytometers (BD), with FACS Diva software.
803
804 ***Atomic force microscopy***
805 $1x10^5$ cells in 2 mL of CGM were plated in a glass bottom dish (World Precision Instruments,
806 FD35-100). 6 hours after treatment with EtOH or TAM in the absence or presence of EGTA,
807 RGM was replaced by CO_2-independent media (Thermo Fisher Scientific 18045054) with
808 EtOH or 4OH-TAM in the presence or absence of EGTA. EGTA induced the appearance of
809 two morphologically distinct cell populations in both EtOH- and TAM-treated cells. The round
810 cell populations were excluded from the analysis, as we assume that these cells are losing
811 adherence to the glass substrate. For the AFM indentation experiments, a Nanowizard 4 (JPK
812 Instruments, Berlin) mounted on top of a light microscope (Zeiss Axiobserver) was used,
813 combined with a petri dish heater to keep the temperature at 37°C during experiments. Arrow-
814 T1 cantilevers (Nanoworld, Neuchatel, Switzerland) were modified with polystyrene beads
815 (radius 2.5 µm, Microparticles GmbH, Berlin, Germany) using epoxy glue to obtain a well-
816 defined spherical indenter geometry and decrease local strain during indentation. The
817 cantilever was lowered over the central part of the cell with a speed of 5 µm s^{-1} until a relative
818 set point of 2.5 nN was reached. Each cell was probed three times in the same location. The
819 resulting force-distance curves were analyzed using JPK image processing software (JPK
820 instruments). Force-distance data were corrected for the tip sample separation and fitted with
821 a Hertz model for a spherical indenter to extract the apparent Young's Modulus within an
822 indentation depth of approximately 1 µm. A Poisson ratio of 0.5 was assumed. The average of
823 the Young's Modulus of the three curves was calculated for each cell. A 2-hour time window
824 was required for measurement of the four experimental conditions.
825
826 ***Quantifications***
827 The NIH Fiji/ImageJ program was used to quantify the ratio of the GFP-positive wing disc area
828 to the total disc area. Comparisons between wing imaginal discs overexpressing Src64B and
829 p35 alone or together with UAS-Ecad-IR were performed using the same number of UAS
830 transgenes. For each wing disc, the area of the GFP domain and the area of the whole disc

831 domain highlighted by Phalloidin staining were outlined manually and measured using the
832 *Area* function, which evaluates size in square pixels. The ratio was calculated for each disc
833 between the two. To quantify the intensity of the α18 staining, maximum intensity Z-
834 projections of the p120ctn and α18 channels were performed for each field using the NIH
835 Fiji/ImageJ program. The segmented line tool was used to overlap the p120ctn signal with the
836 line width set to 10. Each line was then used to measure the mean gray value in the α18 channel.
837 Three fields per condition were quantified for each biological replicate. To quantify FA size,
838 maximum intensity Z-projections of the Zyxin channel were performed for each field using the
839 NIH Fiji/ImageJ program. Images were then segmented using the LABKIT Fiji plugin to
840 generate binary masks. The size of particles was then extracted and displayed in pixel units.
841 To compare the size of FAs between ER-Src cells treated with EtOH or TAM for 6 or 12 hours,
842 images were acquired on a single point scanning confocal SP5, equipped with a fully motorized
843 inverted Leica DMI6000 microscope (Leica Microsystems), with a 63x objective using a zoom
844 factor 3 to analyze FA area between ER-Src cells treated with EtOH or TAM for 6 or 12 hours
845 or a zoom factor 2 to determine the effect of EGTA on the FA area. 3 to 5 fields per condition
846 were quantified for each biological replicate. To analyze FA area between ER-Src cells treated
847 with EtOH or TAM for 6 or 12 hours, particles smaller than 20 pixels were considered
848 nonspecific signals and were excluded. To analyze the effect of EGTA on the FA area, all
849 particles were included. R was used for the statistical analysis of AFM data. GraphPad Prism
850 (10.0) was used for all other statistical analysis and for data presentation.

Acknowledgements

We specially thank K. Struhl, Alex Dunn, G. Posern, A. Nagafuchi, A. Dunn and M. Schwartz for reagents and all members of F.J. lab for helpful discussions. We acknowledge the Cell Culture and Genotyping, the Genomics, the Translational Cytometry, the Bioimaging and the Advanced Light Microscopy platforms at i3S. Stocks obtained from the Bloomington Drosophila Stock Center (NIH P40OD018537) and from the Vienna Drosophila Research Center, VDRC, were used in this study. This research was funded by Fundação para a Ciência e Tecnologia I.P. (FCT), grant number PTDC/BIA-BFS/0812/2021 and 2022.06763.CEECIND to F.J. and PhD fellowship number 2022.11122.BD (doi https://doi.org/10.54499/2022.11122.BD) to L.F. The i3S Bioimaging and Advanced Light Microscopy scientific platforms are both members of the national infrastructure PPBI-Portuguese Platform of BioImaging (POCI-01-0145-FEDER-022122).

Author contributions

Conceptualization F.J.; Methodology F.J., M.A., P.S., A.T.; Investigation, L.F., C.G., I.F.; C.S.L; V.R., S.T., V.M., F.J.; Formal Analysis, L.F., C.G., I.F.; C.S.L; V.R., S.T., V.M., F.J.; Writing – Original Draft, F.J.; Writing – Review & Editing, L.F., C.G., I.F.; C.S.L; V.R., S.T., V.M., F.J.; Funding Acquisition, F.J.; Supervision, F.J., A.T. and L.F.

Disclosure and competing interest statement

The authors of this manuscript declare that they have no conflict of interest and no competing financial interests in relation to the work described. The material of this work is original research.

Data Availability

Correspondence and material requests should be addressed to fjanody@i3s.up.pt.

References

1. Arpino G, Laucirica R, Elledge RM. Premalignant and in situ breast disease: biology and clinical implications. Ann Intern Med **2005**;143:446-57
2. Buyuk B, Jin S, Ye K. Epithelial-to-Mesenchymal Transition Signaling Pathways Responsible for Breast Cancer Metastasis. Cell Mol Bioeng **2022**;15:1-13
3. Angulo-Urarte A, van der Wal T, Huveneers S. Cell-cell junctions as sensors and transducers of mechanical forces. Biochim Biophys Acta Biomembr **2020**;1862:183316
4. Oda H, Takeichi M. Evolution: structural and functional diversity of cadherin at the adherens junction. J Cell Biol **2011**;193:1137-46
5. Ladoux B, Nelson WJ, Yan J, Mege RM. The mechanotransduction machinery at work at adherens junctions. Integr Biol (Camb) **2015**;7:1109-19
6. Nose A, Takeichi M. A novel cadherin cell adhesion molecule: its expression patterns associated with implantation and organogenesis of mouse embryos. J Cell Biol **1986**;103:2649-58
7. Tadokoro S, Shattil SJ, Eto K, Tai V, Liddington RC, de Pereda JM*, et al.* Talin binding to integrin beta tails: a final common step in integrin activation. Science **2003**;302:103-6
8. Carisey A, Tsang R, Greiner AM, Nijenhuis N, Heath N, Nazgiewicz A*, et al.* Vinculin regulates the recruitment and release of core focal adhesion proteins in a force-dependent manner. Curr Biol **2013**;23:271-81
9. Grashoff C, Hoffman BD, Brenner MD, Zhou R, Parsons M, Yang MT*, et al.* Measuring mechanical tension across vinculin reveals regulation of focal adhesion dynamics. Nature **2010**;466:263-6
10. Borghi N, Sorokina M, Shcherbakova OG, Weis WI, Pruitt BL, Nelson WJ*, et al.* E-cadherin is under constitutive actomyosin-generated tension that is increased at cell-cell contacts upon externally applied stretch. Proc Natl Acad Sci U S A **2012**;109:12568-73
11. Zuidema A, Wang W, Sonnenberg A. Crosstalk between Cell Adhesion Complexes in Regulation of Mechanotransduction. Bioessays **2020**;42:e2000119
12. Gjorevski N, Piotrowski AS, Varner VD, Nelson CM. Dynamic tensile forces drive collective cell migration through three-dimensional extracellular matrices. Sci Rep **2015**;5:11458
13. Provenzano PP, Inman DR, Eliceiri KW, Keely PJ. Matrix density-induced mechanoregulation of breast cell phenotype, signaling and gene expression through a FAK-ERK linkage. Oncogene **2009**;28:4326-43
14. Sullivan B, Light T, Vu V, Kapustka A, Hristova K, Leckband D. Mechanical disruption of E-cadherin complexes with epidermal growth factor receptor actuates growth factor-dependent signaling. Proc Natl Acad Sci U S A **2022**;119
15. Martinez-Rico C, Pincet F, Thiery JP, Dufour S. Integrins stimulate E-cadherin-mediated intercellular adhesion by regulating Src-kinase activation and actomyosin contractility. J Cell Sci **2010**;123:712-22
16. Maruthamuthu V, Sabass B, Schwarz US, Gardel ML. Cell-ECM traction force modulates endogenous tension at cell-cell contacts. Proc Natl Acad Sci U S A **2011**;108:4708-13
17. Muhamed I, Wu J, Sehgal P, Kong X, Tajik A, Wang N*, et al.* E-cadherin-mediated force transduction signals regulate global cell mechanics. J Cell Sci **2016**;129:1843-54

927 18. Sehgal P, Kong X, Wu J, Sunyer R, Trepat X, Leckband D. Epidermal growth factor
928 receptor and integrins control force-dependent vinculin recruitment to E-cadherin
929 junctions. J Cell Sci **2018**;131
930 19. Tavares S, Vieira AF, Taubenberger AV, Araujo M, Martins NP, Bras-Pereira C*, et*
931 *al.* Actin stress fiber organization promotes cell stiffening and proliferation of pre-
932 invasive breast cancer cells. Nat Commun **2017**;8:15237
933 20. Faria L, Canato S, Jesus TT, Goncalves M, Guerreiro PS, Lopes CS*, et al.* Activation
934 of an actin signaling pathway in pre-malignant mammary epithelial cells by P-
935 cadherin is essential for transformation. Dis Model Mech **2023**;16
936 21. Selvaggio G, Canato S, Pawar A, Monteiro PT, Guerreiro PS, Bras MM*, et al.* Hybrid
937 Epithelial-Mesenchymal Phenotypes Are Controlled by Microenvironmental Factors.
938 Cancer Res **2020**;80:2407-20
939 22. Padilla-Parra S, Tramier M. FRET microscopy in the living cell: different approaches,
940 strengths and weaknesses. Bioessays **2012**;34:369-76
941 23. Nagafuchi A, Tsukita S. The Loss of the Expression of alpha Catenin, the 102 kD
942 Cadherin Associated Protein, in Central Nervous Tissues during Development: (alpha
943 catenin/cadherin/cell adhesion/CNS). Dev Growth Differ **1994**;36:59-71
944 24. Wang HB, Dembo M, Hanks SK, Wang Y. Focal adhesion kinase is involved in
945 mechanosensing during fibroblast migration. Proc Natl Acad Sci U S A
946 **2001**;98:11295-300
947 25. Horton ER, Humphries JD, James J, Jones MC, Askari JA, Humphries MJ. The
948 integrin adhesome network at a glance. J Cell Sci **2016**;129:4159-63
949 26. Kartenbeck J, Schmid E, Franke WW, Geiger B. Different modes of internalization of
950 proteins associated with adhaerens junctions and desmosomes: experimental
951 separation of lateral contacts induces endocytosis of desmosomal plaque material.
952 EMBO J **1982**;1:725-32
953 27. Kumper S, Ridley AJ. p120ctn and P-cadherin but not E-cadherin regulate cell
954 motility and invasion of DU145 prostate cancer cells. PLoS One **2010**;5:e11801
955 28. Wei SY, Escudero LM, Yu F, Chang LH, Chen LY, Ho YH*, et al.* Echinoid is a
956 component of adherens junctions that cooperates with DE-Cadherin to mediate cell
957 adhesion. Dev Cell **2005**;8:493-504
958 29. Bosch-Fortea M, Martin-Belmonte F. Mechanosensitive adhesion complexes in
959 epithelial architecture and cancer onset. Curr Opin Cell Biol **2018**;50:42-9
960 30. Montemurro M, Monier B, Suzanne M. The mechanical state of pre-tumoral epithelia
961 controls subsequent Drosophila tumor aggressiveness. Dev Cell **2025**;60:1036-52 e7
962 31. de Rooij J, Kerstens A, Danuser G, Schwartz MA, Waterman-Storer CM. Integrin-
963 dependent actomyosin contraction regulates epithelial cell scattering. J Cell Biol
964 **2005**;171:153-64
965 32. Rolland Y, Marighetti P, Malinverno C, Confalonieri S, Luise C, Ducano N*, et al.*
966 The CDC42-interacting protein 4 controls epithelial cell cohesion and tumor
967 dissemination. Dev Cell **2014**;30:553-68
968 33. Kuwahara K, Kinoshita H, Kuwabara Y, Nakagawa Y, Usami S, Minami T*, et al.*
969 Myocardin-related transcription factor A is a common mediator of mechanical stress-
970 and neurohumoral stimulation-induced cardiac hypertrophic signaling leading to
971 activation of brain natriuretic peptide gene expression. Mol Cell Biol **2010**;30:4134-
972 48
973 34. Yano S, Komine M, Fujimoto M, Okochi H, Tamaki K. Mechanical stretching in
974 vitro regulates signal transduction pathways and cellular proliferation in human
975 epidermal keratinocytes. J Invest Dermatol **2004**;122:783-90

35. Pece S, Gutkind JS. Signaling from E-cadherins to the MAPK pathway by the recruitment and activation of epidermal growth factor receptors upon cell-cell contact formation. J Biol Chem **2000**;275:41227-33
36. Lysne D, Johns J, Walker A, Ecker R, Fowler C, Lawson KR. P-cadherin potentiates ligand-dependent EGFR and IGF-1R signaling in dysplastic and malignant oral keratinocytes. Oncol Rep **2014**;32:2541-8
37. Bazellieres E, Conte V, Elosegui-Artola A, Serra-Picamal X, Bintanel-Morcillo M, Roca-Cusachs P*, et al.* Control of cell-cell forces and collective cell dynamics by the intercellular adhesome. Nat Cell Biol **2015**;17:409-20
38. Ribeiro AS, Sousa B, Carreto L, Mendes N, Nobre AR, Ricardo S*, et al.* P-cadherin functional role is dependent on E-cadherin cellular context: a proof of concept using the breast cancer model. J Pathol **2013**;229:705-18
39. Ribeiro AS, Carvalho FA, Figueiredo J, Carvalho R, Mestre T, Monteiro J*, et al.* Atomic force microscopy and graph analysis to study the P-cadherin/SFK mechanotransduction signalling in breast cancer cells. Nanoscale **2016**;8:19390-401
40. Taniuchi K, Nakagawa H, Hosokawa M, Nakamura T, Eguchi H, Ohigashi H*, et al.* Overexpressed P-cadherin/CDH3 promotes motility of pancreatic cancer cells by interacting with p120ctn and activating rho-family GTPases. Cancer Res **2005**;65:3092-9
41. Cheung LW, Leung PC, Wong AS. Cadherin switching and activation of p120 catenin signaling are mediators of gonadotropin-releasing hormone to promote tumor cell migration and invasion in ovarian cancer. Oncogene **2010**;29:2427-40
42. Rao TC, Ma VP, Blanchard A, Urner TM, Grandhi S, Salaita K*, et al.* EGFR activation attenuates the mechanical threshold for integrin tension and focal adhesion formation. J Cell Sci **2020**;133
43. Moro L, Venturino M, Bozzo C, Silengo L, Altruda F, Beguinot L*, et al.* Integrins induce activation of EGF receptor: role in MAP kinase induction and adhesion-dependent cell survival. EMBO J **1998**;17:6622-32
44. Clarke DN, Miller PW, Martin AC. EGFR-dependent actomyosin patterning coordinates morphogenetic movements between tissues in Drosophila melanogaster. Dev Cell **2025**;60:270-87 e6
45. Chan MW, Arora PD, Bozavikov P, McCulloch CA. FAK, PIP5KIgamma and gelsolin cooperatively mediate force-induced expression of alpha-smooth muscle actin. J Cell Sci **2009**;122:2769-81
46. Kruse K, Komarova YA. Tension across adherens junctions: when less is more. Oncotarget **2015**;6:30433-4
47. Mendonsa AM, Na TY, Gumbiner BM. E-cadherin in contact inhibition and cancer. Oncogene **2018**;37:4769-80
48. Hirsch HA, Iliopoulos D, Tsichlis PN, Struhl K. Metformin selectively targets cancer stem cells, and acts together with chemotherapy to block tumor growth and prolong remission. Cancer Res **2009**;69:7507-11
49. Posern G, Sotiropoulos A, Treisman R. Mutant actins demonstrate a role for unpolymerized actin in control of transcription by serum response factor. Mol Biol Cell **2002**;13:4167-78